

## RESEARCH ARTICLE

# Ankyrin-G induces nucleoporin Nup358 to associate with the axon initial segment of neurons

Bouchra Khalaf<sup>1</sup>, Alessandro Roncador<sup>1</sup>, Francesca Pischedda<sup>2</sup>, Antonio Casini<sup>3</sup>, Sabine Thomas<sup>4</sup>, Giovanni Piccoli<sup>2</sup>, Michael Kiebler<sup>4</sup> and Paolo Macchi<sup>1,\*</sup>

## ABSTRACT

Nup358 (also known as RanBP2) is a member of the large nucleoporin family that constitutes the nuclear pore complex. Depending on the cell type and the physiological state, Nup358 interacts with specific partner proteins and influences distinct mechanisms independent of its role in nucleocytoplasmic transport. Here, we provide evidence that Nup358 associates selectively with the axon initial segment (AIS) of mature neurons, mediated by the AIS scaffold protein ankyrin-G (AnkG, also known as Ank3). The N-terminus of Nup358 is demonstrated to be sufficient for its localization at the AIS. Further, we show that Nup358 is expressed as two isoforms, one full-length and another shorter form of Nup358. These isoforms differ in their subcellular distribution in neurons and expression level during neuronal development. Overall, the present study highlights an unprecedented localization of Nup358 within the AIS and suggests its involvement in neuronal function.

This article has an associated First Person interview with the first author of the paper.

**KEY WORDS:** Nucleoporin, RanBP2, Nup358, Ankyrin-G, Axon initial segment

## INTRODUCTION

The nuclear pore complex (NPC) is a large multiprotein complex that traverses the nuclear envelope and provides a channel through which RNA and proteins travel between the nucleus and the cytoplasm (Chatel and Fahrenkrog, 2012; D'Angelo and Hetzer, 2006). The overall structure comprises multiple copies of ~30 different proteins termed nucleoporins (Cronshaw et al., 2002; Reichelt et al., 1990; Suntharalingam and Wentz, 2003; Yang et al., 1998). In eukaryotic cells, nucleoporins are primarily detected at the nuclear rim owing to their association with the NPC; however, a few studies have shown that individual nucleoporins can also be present in the cytoplasm and/or the nucleoplasm and contribute to numerous physiological events (Bodoor et al., 1999; Chatel and Fahrenkrog, 2012; Griffis et al., 2002; Guan et al., 2000; Rabut et al., 2004).

Nup358, also known as Ran-binding protein 2 (RanBP2), is by far the largest nucleoporin with an approximate molecular mass of 358 kDa (Bernad et al., 2004; Delphin et al., 1997; Yokoyama et al., 1995). It harbors several distinct domains: an N-terminus of ~700-residues, known as the leucine-rich region (LRR), containing a leucine zipper motif, four homologous RanGTP-binding domains, eight tandem zinc finger motifs, a small ubiquitin-like modifier (SUMO) E3 ligase domain, and a C-terminal cyclophilin A homology domain (Wu et al., 1995). Because of this multi-domain architecture, Nup358 interacts with specific cellular proteins and consequently triggers a range of downstream effects. For instance, during mitosis Nup358 relocates to microtubules (MTs) and mediates their stability and interaction with kinetochores (Dawlaty et al., 2008; Hashizume et al., 2013; Joseph et al., 2004; Salina et al., 2003). In the mouse retina, Nup358 localizes to the mitochondria-rich ellipsoid compartment of cone and rod photoreceptors and associates with Cox11 through its LRR (Aslanukov et al., 2006; Mavlyutov et al., 2002). In developing neurons, Nup358 regulates axon specification and neuronal polarity through an interaction with dishevelled and aPKC proteins (Vyas et al., 2013). However, in mature neurons, the localization pattern and function of Nup358 are poorly characterized.

Here, we report a unique subcellular distribution of Nup358, present not only at the nuclear rim associated with NPCs but also in the cell body associated with the endoplasmic reticulum (ER) and remarkably enriched at the axon initial segment (AIS) of mature neurons. Because the AIS is a highly specialized region of neuronal cells responsible for maintaining neuronal polarity and action potential generation (Grubb and Burrone, 2010b; Leterrier and Dargent, 2014; Yoshimura and Rasband, 2014), the highlight of the present study is identifying nucleoporin Nup358 as a previously unknown component of the AIS, dependent on the master AIS scaffold, ankyrin-G (AnkG, also known as Ank3). We examined the protein expression of Nup358 during neuronal development and showed that Nup358 is present as two isoforms: one full-length and another shorter form that is predominantly expressed in mature neurons. Next, we studied the correlation between neuronal activity and Nup358 protein level and subcellular distribution, and demonstrated that stimulating neuronal activity with pharmacological drugs results in a decrease in Nup358 protein levels without interfering with the Nup358 pool at the AIS. Overall, our findings provide an insight into how Nup358 associates with the AIS and imply its specialized function in neurons that requires further examination.


## RESULTS

### Nup358 associates with the AIS

We first examined the subcellular localization of Nup358 in neuronal cells. At 14 days *in vitro* (DIV), mouse cortical neurons were immunostained for Nup358 and  $\beta$ III-tubulin (also known as Tubb3), a neuron-specific marker for microtubules. As expected, Nup358 decorated the boundaries of cell nuclei as a result of its association

<sup>1</sup>Laboratory of Molecular and Cellular Neurobiology, Department of Cellular, Computational and Integrative Biology-CIBIO, University of Trento, 38123 Trento, Italy. <sup>2</sup>Dulbecco Telethon Laboratory of Biology of Synapses, Department of Cellular, Computational and Integrative Biology-CIBIO, University of Trento, 38123 Trento, Italy. <sup>3</sup>Laboratory of Molecular Virology, Department of Cellular, Computational and Integrative Biology-CIBIO, University of Trento, 38123 Trento, Italy. <sup>4</sup>Department for Cell Biology, Biomedical Center, Medical Faculty, Ludwig-Maximilian University of Munich, Großhaderner Straße 9, 82152 Planegg-Martinsried, Germany.

\*Author for correspondence (paolo.macchi@unitn.it)

 B.K., 0000-0002-5665-1043; P.M., 0000-0002-7245-9019

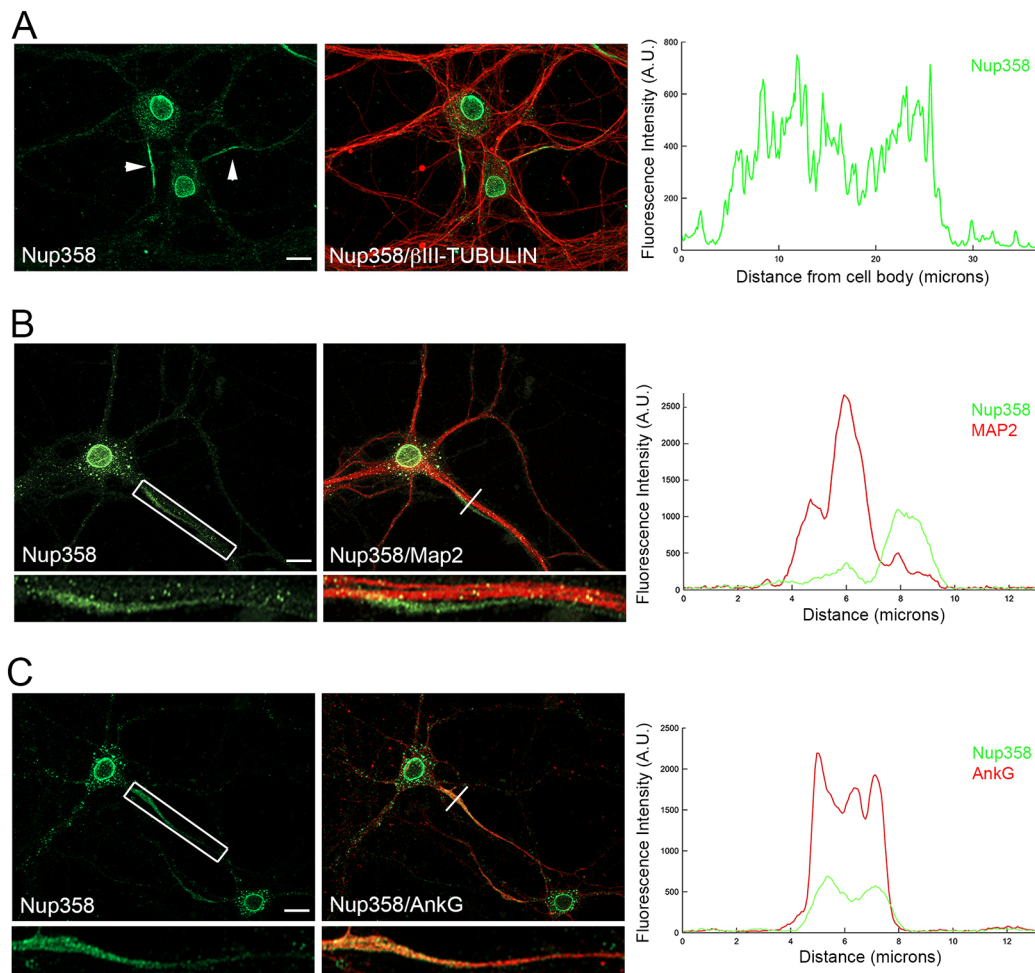


**Fig. 1. Nup358 is targeted to the AIS of mature neurons.** 14 days *in vitro* (DIV) mouse cortical neurons co-immunostained for Nup358 and (A) βIII-tubulin, (B) MAP2 and (C) AnkG. Arrowheads in A mark the high intensity of Nup358 in specific regions of the neuronal network. At the bottom of panels B and C are magnified views of the corresponding boxed areas. Accompanying graphs are line scan analyses of Nup358 fluorescence intensity (arbitrary units, A.U.) along the AIS in A, or along the white lines in B and C, demonstrating an overlap between Nup358 and AnkG peaks but not with those of MAP2. Scale bars: 10 μm.

with NPCs at the nuclear envelope (Fig. 1A). This perinuclear localization of Nup358 was confirmed by co-staining with the NPC protein marker, monoclonal antibody mAb414, which recognizes the FXFG repeat sequence in nucleoporins (Davis and Blobel, 1986) (Fig. S1A). Additionally, Nup358 had a punctate pattern in the soma and neuronal processes and was, remarkably, enriched in the proximal region (5–30 μm away from the cell body) of one process per individual neuronal cell (Fig. 1A, arrowheads). This region that resembled the AIS was validated as such since Nup358 was more pronounced in the processes where dendritic marker MAP2 signal was excluded (Fig. 1B), but overlapping with staining for AIS marker AnkG (Fig. 1C). Next, we assessed whether the cytoplasmic puncta of Nup358 lie within any of the major subcellular compartments and organelles. We immunostained neurons for the following markers: calnexin (CLX, also known as Canx) for the ER, p58 as *cis*-Golgi marker (Saraste et al., 1987), and COX1 as marker for mitochondria (Dennerlein and Rehling, 2015). Nup358 was found associated with the ER (Fig. 2A), in juxtaposition with the Golgi (Fig. 2B) and absent from mitochondria (Fig. 2C). These observations were confirmed quantitatively with Manders' coefficients after thresholding that indicate moderate colocalization of Nup358 and the ER marker with mean  $tM1=0.88$  for Nup358–CLX and mean  $tM2=0.77$  for CLX–Nup358. In contrast, Nup358 colocalization coefficient with either the

Golgi or mitochondria marker was below 0.6 (no colocalization) (Fig. 2D).

Nup358 expression in areas other than the nuclear envelope has previously been reported in different cell types (Cordes et al., 1996; Raghunayakula et al., 2015; Sahoo et al., 2017). However, Nup358 was almost always detected together with other nucleoporins in structures known as annulate lamellae (AL), which are cytoplasmic organelles composed of ER membranous sheets with embedded pore complexes (Kessel, 1992). In our neuronal cultures, AL, identified as mAb414-immunolabeled dots in the cytoplasm, were scarce compared to the cytoplasmic puncta of Nup358 (see Fig. S1A). This was further confirmed by immunostaining neurons for specific nucleoporins known to be incorporated into AL such as Nup98 (Miller and Forbes, 2000) and more importantly, Nup88 (Wu et al., 2001) that interacts with Nup358 at the cytoplasmic side of the NPC (Bernad et al., 2004) (Fig. S1B,C). Moreover, because Nup358 binds to Ran and RanGAPs (Mahajan et al., 1997; Yokoyama et al., 1995), both of which are key players in nucleocytoplasmic transport, we examined possible relocation of these molecular partners with Nup358 to the AIS or cytoplasmic puncta (Fig. S2A). However, neither protein overlapped with Nup358 in subcellular regions other than the nuclear rim. Taken together, these data show that in neurons,

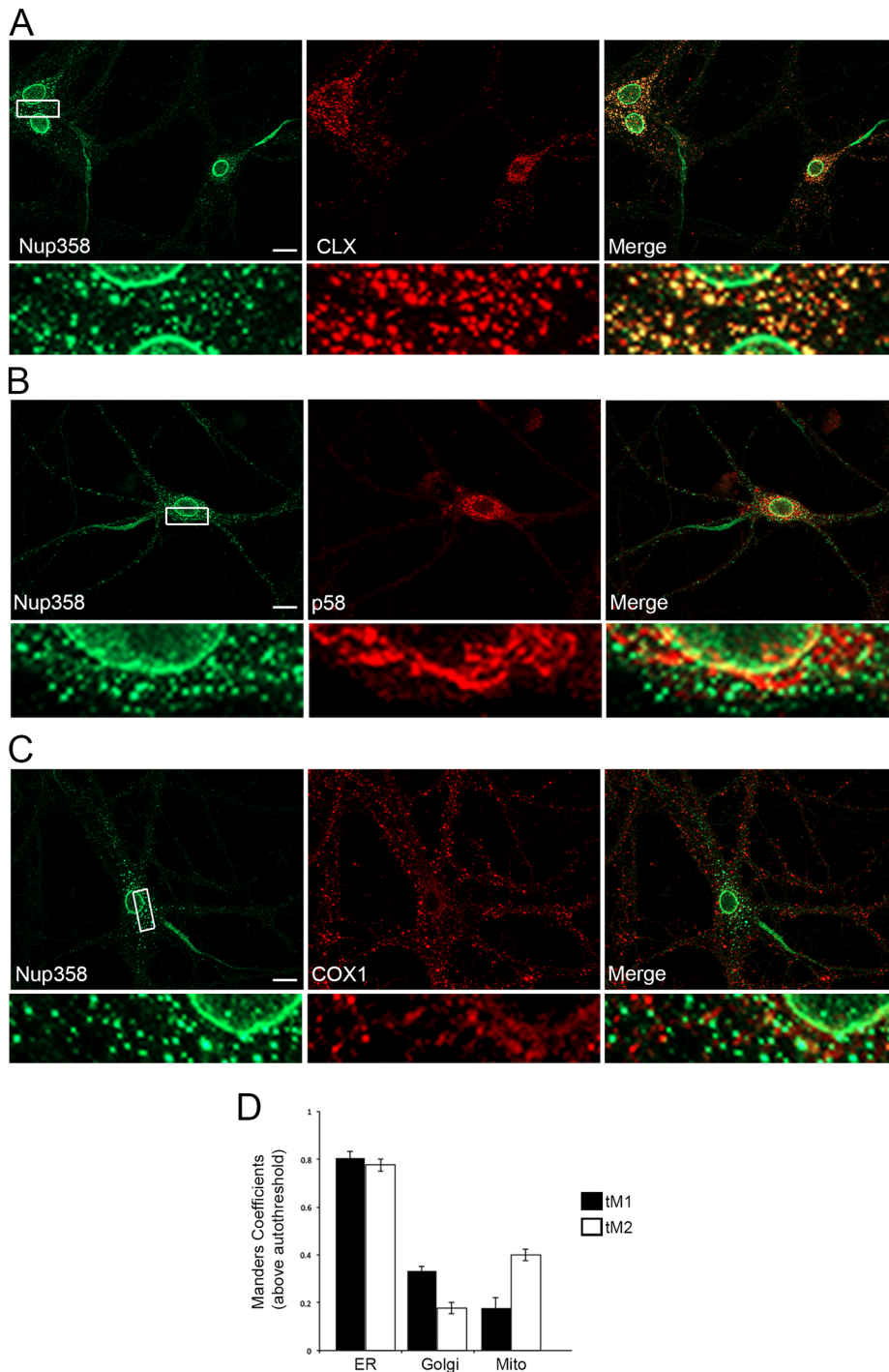


**Fig. 2. The somatodendritic puncta of Nup358 localize at the endoplasmic reticulum.**

(A–C) 14 DIV cortical neurons co-immunostained for Nup358 and the following markers: calnexin (CLX) as a marker for the endoplasmic reticulum (A), p58 for the Golgi apparatus (B), and cytochrome c oxidase I (COX1) for mitochondria (C). Magnified views of boxed areas are shown at the bottom of the panels. Scale bars: 10  $\mu$ m. (D) Analysis of Nup358 colocalization with the endoplasmic reticulum (ER), Golgi or mitochondria (Mito) markers using thresholded Manders' coefficients (tM1 and tM2). tM1 is the thresholded coefficient of Nup358 fluorescence intensity colocalizing with CLX, p58 or COX1, i.e. Nup358:CLX, Nup358:p58 or Nup358:COX1. Conversely, tM2 is the thresholded coefficient of CLX, p58 or COX1 colocalizing with Nup358, i.e. CLX:Nup358, p58:Nup358 or COX1:Nup358. The results represent mean $\pm$ s.e.m from two independent experiments, where the number of cells analyzed is  $n=23$ , 34, and 31 for each of the ER, Golgi, and mitochondria, respectively.

Nup358 has a distribution profile distinct from those of other nucleoporins or its molecular partners.

The NPC mediates the nucleocytoplasmic transport of molecules including RNA. Individual nucleoporins such as Nup98 and Nup153 interact with transcribed RNA molecules and assist their export to the cytoplasm; hence, their mobility and association with the NPC are transcription-dependent (Griffis et al., 2004). In this context, we examined whether RNA transcription would similarly influence the intracellular distribution of Nup358. Cortical neurons at 14 DIV were treated with actinomycin D (ActD) to inhibit RNA transcription. To verify the efficiency of ActD treatment, neurons were incubated with 5-ethynyl uridine, a uracil analog that is

incorporated into nascent RNA during active transcription and can be detected with a click reaction using the fluorescent dye 5-FAM (Fig. S2B). Compared to control neurons (vehicle-treated), ActD-treated neurons showed a very low signal for active transcription but exhibited similar subcellular localization of Nup358 (Fig. S2B,C), thus ruling out the role of RNA transcription in regulating the redistribution of the Nup358 pool.

#### AnkG induces Nup358 to associate with the AIS

Although Nup358 localization at the ER and generally its punctate pattern in the cell body and neuronal processes were worthy of further investigation, we focused instead on Nup358 association with the

AIS as it is a highly specialized structure in neurons and is crucial for maintaining neuronal polarity and the generation of action potentials (Leterrier, 2018). To examine Nup358 expression during AIS formation, cultured mouse cortical neurons were fixed at different days *in vitro* (1–7 DIV and 14 DIV) and co-immunostained for Nup358 and AnkG. Co-immunostaining for AnkG was chosen for two main reasons: first, AnkG is one of the early markers of AIS formation (Grubb and Burrone, 2010b); second, AnkG is crucial for the concentration of other AIS proteins including voltage-gated

sodium and potassium channels (Pan et al., 2006; Rasmussen et al., 2007), and the cell adhesion molecules NrCAM and neurofascin (Nfasc) isoform NF-186 (Hedstrom et al., 2008). As early as 1 DIV, Nup358 exhibited a punctate pattern in the cell body (Fig. 3A, 1 DIV) that enhanced progressively as neurons developed in culture (Fig. 3A, 5 DIV). However, Nup358 was only notably detected at the AIS following an earlier expression of AnkG (Fig. 3A, 5 and 7 DIV, arrowheads). Subsequently, at 14 DIV the Nup358 distribution profile consisted of three identified pools: one pool localized at the

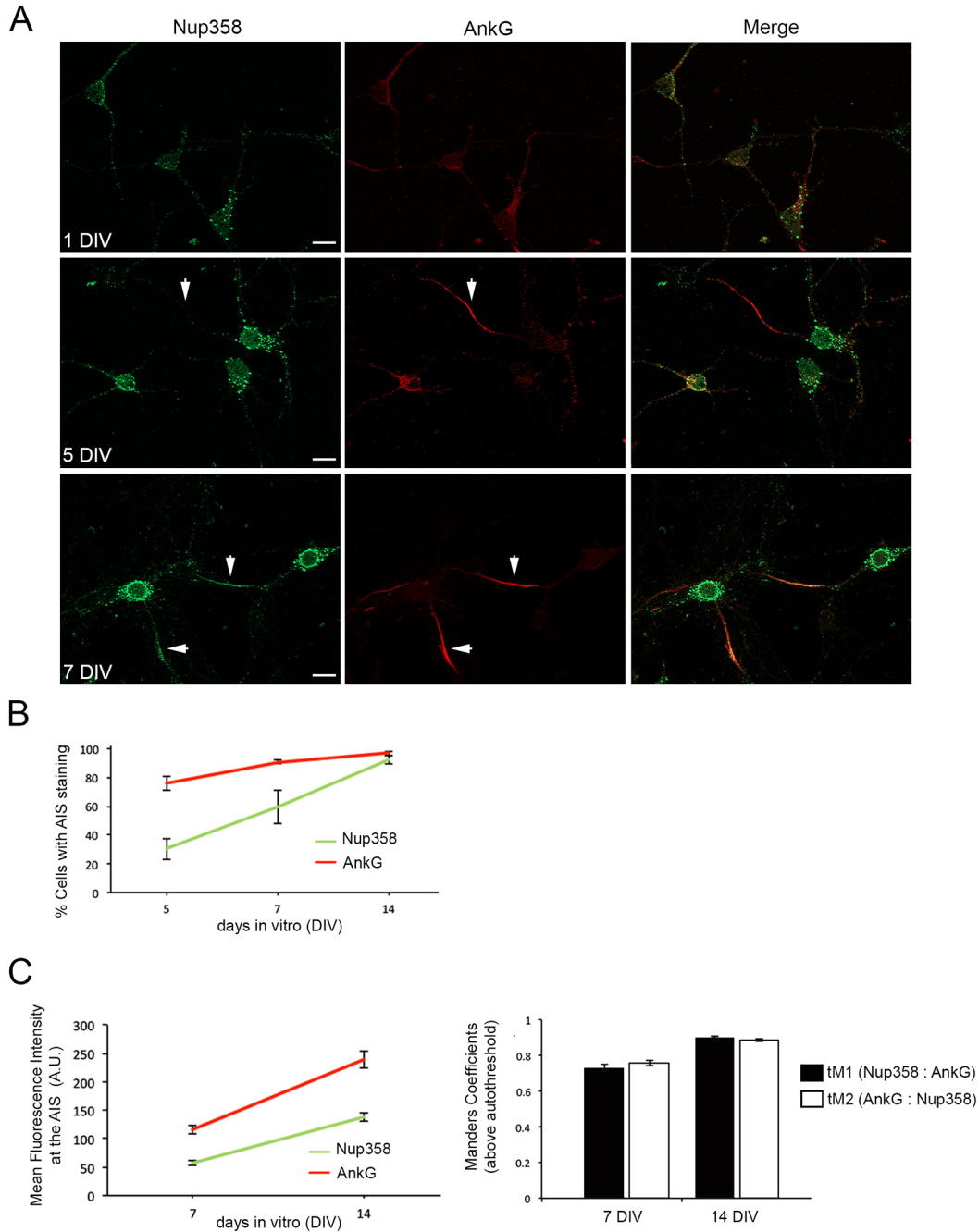


**Fig. 3. AnkG targets Nup358 to the AIS of developing neurons.** (A) Mouse cortical neurons were immunostained for Nup358 and AnkG. The arrows point to the recruitment of Nup358 and/or AnkG to the AIS. Scale bars: 10  $\mu$ m. (B) Percentage of neurons expressing Nup358 and/or AnkG at the AIS during *in vitro* development. The results are mean  $\pm$  s.e.m. of three independent experiments with  $n=144$  (5 DIV),  $n=157$  (7 DIV) and  $n=146$  (14 DIV). (C) Quantitative analysis of Nup358 and AnkG mean fluorescence intensities at the AIS (arbitrary units, A.U.). The histogram validates Nup358 colocalization with AnkG at the AIS using thresholded Manders' coefficients. tM1 represents Nup358:AnkG while tM2 represents AnkG:Nup358. The results are mean  $\pm$  s.e.m. of two independent experiments. The number of cells analyzed is  $n=45$  at 7 DIV and  $n=56$  at 14 DIV.

nuclear rim associated with NPCs, another was present as discrete spots in the cell soma and the processes, and a third pool was enriched at the AIS (see Fig. 1). We then confirmed that AnkG precedes Nup358 in expression at the AIS. At a premature stage (5 DIV), the majority of neurons expressed AnkG compared to  $30.35 \pm 7.38\%$  (mean  $\pm$  s.e.m.) cells expressing Nup358 at the AIS (Fig. 3B). Despite their temporal expression at the AIS, both Nup358 and AnkG fluorescence intensities increased as neurons developed from 7 to 14 DIV, with their colocalization coefficient increasing relatively (Fig. 3C).

Nup358 expression and colocalization with AnkG in cultured neurons prompted us to investigate a possibly similar scenario in isolated nervous tissues. To this end, we chose to immunostain sections of mouse retina against both proteins since the retina is an extension of the brain and it comprises a thin sheet of non-myelinated nervous tissue. Nup358 was poorly to moderately detected around cell nuclei of the outer and inner nuclear layers, respectively (ONL and INL). In the ganglion cell layer (GCL), Nup358 was more abundant and exhibited a bright signal at the nuclear rim of ganglion cells (Fig. S3A) in agreement with an earlier study (Mavlyutov et al., 2002). Nup358 was also prominent in the region between the ONL and the INL. Above all and in support of our earlier hypothesis, a partial overlap was observed between Nup358 and AnkG in the inner plexiform layer (IPL) where cells of the INL synapse with ganglion cells of the GCL (Fig. S3A, arrowheads). Next, because the AIS and nodes of Ranvier (NOR) are both electrically excitable domains that share a similar composition of ion channels, cytoskeletal and scaffold proteins (Nelson and Jenkins, 2017), we assessed whether Nup358 is also expressed at NOR. Sections of the sciatic nerve were immunostained for Nup358 and neurofascin, a protein that associates with both the AIS and NOR (Hedstrom et al., 2007; Sherman et al., 2005) or CASPR (also known as Cntnap), a protein family present in the paranodal regions, the regions present at both sides of the NOR (Einheber et al., 1997). Surprisingly, Nup358 signal was present at NOR and extended to the paranodes (Fig. S3B,C); nonetheless, Nup358 expression at the paranodes highlights its unknown non-canonical role beyond the NPC.

The spatiotemporal distribution profiles of Nup358 and AnkG suggest a role of AnkG in targeting Nup358 to the AIS (see Fig. 3). To investigate the Nup358–AnkG interrelationship, either protein was downregulated using RNA interference in developing cortical neurons. As negative control, neurons were transfected with a non-targeted sh-CTRL construct. The efficiency of shRNAs in eliminating the target protein was evaluated by immunostaining (Fig. 4A) and western blotting analysis (Fig. S4A). In AnkG-depleted neurons, Nup358 failed to concentrate at the AIS and its expression was limited to the nuclear rim and throughout the soma (Fig. 4A, sh-AnkG). A  $70.51 \pm 4.19\%$  (mean  $\pm$  s.e.m.) decrease in AnkG immunoreactivity corresponded to a  $75.24 \pm 4.01\%$  decrease in Nup358 fluorescence intensity at the AIS. Conversely, when Nup358 signal at the AIS was downregulated to  $51.58 \pm 2.64\%$ , AnkG fluorescence intensity at the AIS was reduced by  $68.15 \pm 5.37\%$  compared to non-transfected control cells (Fig. 4A, sh-Nup358). These data thus suggest an interdependent relationship between Nup358 and AnkG; AnkG is a key scaffold for the recruitment of Nup358 to the AIS while Nup358 is equally essential for the enrichment and/or long-term stability of AnkG at this specific region. Additionally, these results verified the specificity of the anti-Nup358 antibody and the selective localization of Nup358 at the AIS.

Next, we assessed whether Nup358 associates with the AIS cytoskeleton. This hypothesis was initially evaluated by testing Nup358 resistance to non-ionic detergent extraction. Being insoluble to detergent extraction is a characteristic feature of most AIS proteins owing to either their direct association with the AIS

cytoskeleton or, indirectly, through the interaction with scaffolding proteins in this region (Sánchez-Ponce et al., 2012; Winckler et al., 1999). Neurons at 14 DIV were treated with 1% Triton X-100 for 5 min before being fixed and immunostained. Nup358 signal was lost from the soma but retained, together with AnkG, at the nuclear rim and at the AIS (Fig. S4B). We tested a more stringent extraction by prolonging the treatment duration to 24 min and as a measure of the efficiency of extraction, neurons were co-immunolabeled for  $\beta$ II-spectrin (also known as Sptbn1), which displays higher expression in the distal axon than at the AIS (Galiano et al., 2012; Zhong et al., 2014). Indeed,  $\beta$ II-spectrin was washed out with Triton X-100 treatment, while Nup358 was detected exclusively at the AIS (Fig. S4C). Next, we examined whether altering the integrity of actin filaments using cytochalasin D (CytoD) or disrupting microtubule polymerization using nocodazole (Noc) would affect the localization of Nup358 at the AIS. Nup358 signal at the AIS was remarkably unaffected in response to either treatment (Fig. 4B,C). These observations were confirmed quantitatively using Operetta high-content analysis that showed no difference in Nup358 fluorescence intensity between CytoD- or Noc-treated neurons and control neurons (Fig. S4D). Taken together, these data indicate that Nup358 localization at the AIS does not depend on the neuronal cytoskeleton, but rather on AnkG as an AIS scaffold protein.

### Two isoforms of Nup358 protein are differentially expressed during neuronal development

Through biochemical analysis, we examined the expression level of Nup358 in cortical neurons cultured for different numbers of days *in vitro* (7, 14 and 21 DIV). To immunoblot for Nup358, we used the same antibody as earlier for the immunostaining (defined from this point forward as Ab-1), which recognizes a region corresponding to amino acid residues 1050–1100 of human Nup358 (see Fig. 6B), and the results were normalized to actin expression levels. Nup358 protein was detected in 7 DIV neurons and expression levels increased progressively during development; however, the band detected was lower than the reported molecular mass of mouse Nup358, which is 341 kDa (Fig. 5A,B, Nup358S). Interestingly, a higher band was weakly detected at this approximate molecular mass; thus, we used another antibody (Ab-2) that proved to have higher affinity for this band and whose recognition site is between amino acids 1–300 of Nup358 protein (see Fig. 6B). Using antibody Ab-2, full-length Nup358 was detected at all time points and had a slightly increasing trend (Fig. 5A,B, Nup358L). Next, we extended our analysis of Nup358 protein expression during *in vivo* development of neurons. We collected cortices from mice of different ages, at embryonic day (E)18 and at a range across postnatal days (P)3–90, and examined protein levels of Nup358. The results showed an increase in expression of the shorter form of Nup358 and an opposite gradual decrease in the full-length form (Fig. 5C,D).

Given that the composition of the NPC changes during neuronal development or differentiation (Lupu et al., 2008; D'Angelo et al., 2012), we sought to examine how expression of nucleoporins varies relative to the changes in Nup358 isoform expression. To this end, protein samples from E18 to P90 mouse cortices were immunoblotted for nucleoporins present in different regions of the NPC: Nup153, of the nuclear basket structure (Sukegawa and Blobel, 1993); Nup98, present in the center of the NPC (Chatel et al., 2012; Krull et al., 2004); and Nup88, localized at the cytoplasmic filaments together with Nup358 (Bernad et al., 2004; Fornerod et al., 1997). In agreement with previous studies, the expression levels of individual nucleoporins were seen to vary independently of each other (Lupu et al., 2008; D'Angelo et al.,

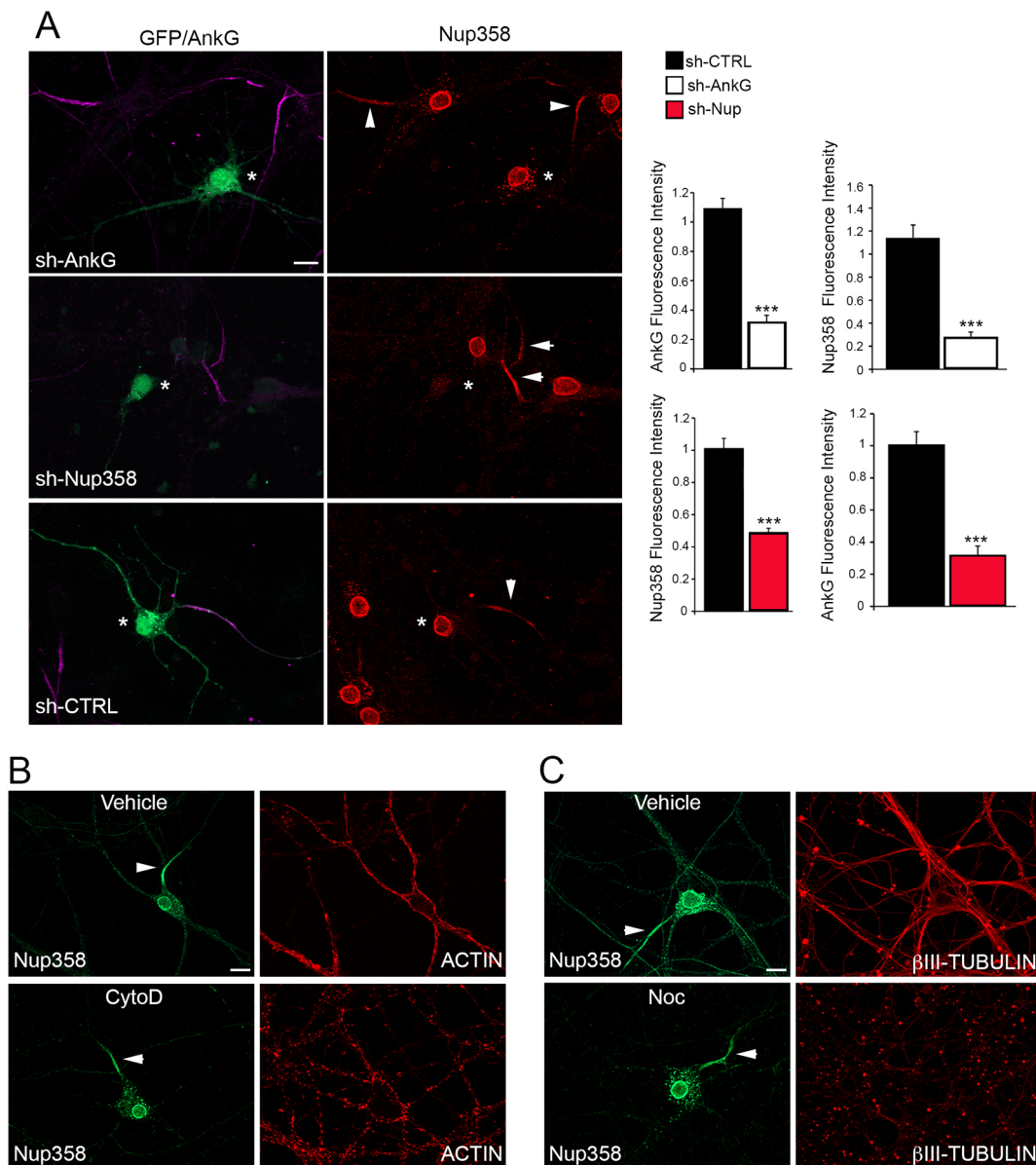


**Fig. 4. Nup358 depends on AnkG for localization at the AIS.** (A) 5 DIV cortical neurons were transfected with shRNA constructs, co-expressing GFP, to downregulate AnkG (sh-AnkG) or Nup358 (a mix of shRNA constructs against Nup358; sh-Nup358) and maintained afterward in culture up to 10 DIV. As control, neurons were transfected with a non-targeted shRNA construct (sh-CTRL). Immunostaining was conducted against AnkG (magenta) and Nup358 (red). Asterisks are used to mark the transfected neuronal cells (green). The graphs represent quantitative analysis of endogenous AnkG and Nup358 proteins at the AIS upon downregulation with the corresponding sh-RNAs. Fluorescence intensity is expressed as mean intensity (MI) reported in GFP-positive cells over MI measured in untransfected cells present in the same field. The results are mean  $\pm$  s.e.m. of three independent experiments. Ten images per each condition were analyzed. \*\*\* $P < 0.001$  (two-tailed Student's *t*-test). (B,C) Immunofluorescence images of neurons treated with cytochalasin D (CytoD; 10  $\mu$ M, 1 h) (B) or nocodazole (Noc; 20  $\mu$ M, 3 h) (C), or with an equivalent amount of DMSO (vehicle) as control. Disruption of actin filaments is monitored by phalloidin staining (red), and depolymerization of microtubules is detected by immunolabeling for the microtubule marker  $\beta$ III-tubulin (red). Arrowheads point to the AIS with a persistent signal of Nup358 (green). Scale bars: 10  $\mu$ m.

2012; Toda et al., 2017), with a decrease in Nup98 and Nup153 (Fig. 5E,F) (Toda et al., 2017) and no apparent change in Nup88 (Fig. 5E,F) and Nup107 (Toda et al., 2017). Such changes in the expression of specific nucleoporins play an important role in cellular function (Toda et al., 2017). Moreover, the increased expression of Nup210 is essential for myogenic and neuronal differentiation (D'Angelo et al., 2012). Thus, our data showing different trends in expression of Nup358 isoforms (see Fig. 5C,D) suggest that each isoform has a distinct function in the early and late developmental stages of neurons that is not necessarily related to nucleocytoplasmic transport.

To determine whether Nup358 is ubiquitously expressed in the central nervous system, we isolated different tissues, e.g. entire brain, hippocampus, cortex and spinal cord tissues from mice at a fixed stage of development and processed samples for western blotting analysis. All tested tissues expressed the two isoforms of Nup358 (Fig. S5A). Moreover, similar to the cortex, developing hippocampus and spinal cord exhibited an increase in expression of the short form of Nup358 and an opposite decrease in the full-length form (Fig. S5B–D). Additionally, in 14 DIV cultured hippocampal neurons, Nup358 localized at the perinuclear region, cell body and the AIS (Fig. S5E) with AnkG being concentrated at this region prior to Nup358 (data not

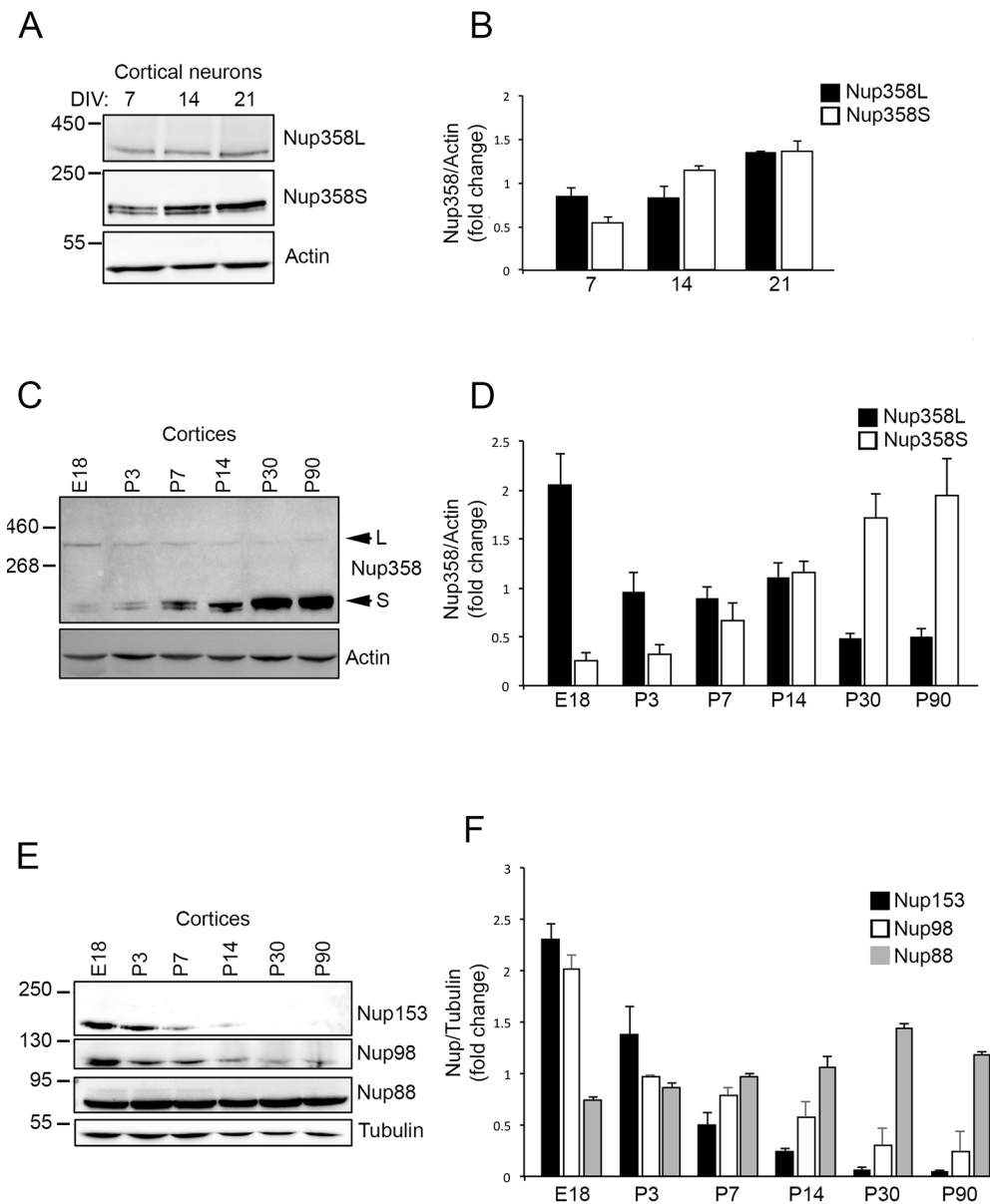


**Fig. 5. Developmental changes in expression of Nup358 protein isoforms.** (A) Immunoblots of Nup358 and actin from cortical neurons cultured for different time intervals (7–21 DIV). Nup358 is detected as two isoforms with varying molecular mass. Nup358L, full-length form (~358 kDa); Nup358S, shorter form (~250 kDa). (B) Densitometric quantifications of Nup358L and Nup358S bands, shown in A, versus actin. (C) Immunoblots of Nup358 and actin from mouse cortices obtained at different ages (embryonic day E18 and the postnatal period P3–P90). (D) Quantifications of Nup358 isoforms:actin ratio in the developing cortex. (E) Immunoblots of the nucleoporins Nup153, Nup98 and Nup88 from developing mouse cortices (E18–P90); tubulin serves as a loading control. Molecular mass markers (kDa) shown to the left of A,C,E. (F) Quantifications of expression of nucleoporins versus tubulin during the development of the mouse cortex from E18 to P90. The results shown are mean  $\pm$  s.e.m. of three independent experiments.

shown). Taking into account these immunocytochemistry and biochemical analyses, we show that Nup358 is ubiquitously present in the CNS and is expressed as two isoforms that are differently modulated during neuronal development.

Apart from an 80 kDa predicted isoform in mitochondria (Patil et al., 2017), no other Nup358 isoform has been previously reported. Thus, we aimed to prove that the 230 kDa band observed in our immunoblots represents an isoform of Nup358. Nup358 was immunoprecipitated from P30 mouse cortex, run on an SDS-PAGE gel and immunoblotted for Nup358 to verify the efficiency of immunoprecipitation (Fig. S5F). Alternatively, the 230 kDa band was detected by Coomassie Blue staining and subsequently analyzed by mass spectrometry (MS). The resulting analysis identified 40 unique peptides for Nup358 and, interestingly enough, two AIS proteins with molecular masses within close range to 230 kDa were identified together with the

immunoprecipitated Nup358, namely neurofascin (186 kDa) and AnkG (270 kDa isoform) (Table S1). To investigate where each isoform of Nup358 is preferentially located, e.g. in the nuclear rim or the cytoplasm including the AIS, we performed nucleo-cytoplasmic fractionation (Benvegnù et al., 2017). The efficiency of fractionation was verified by immunoblotting against the nuclear marker lamin B1, and the cytoplasmic markers GAPDH and tubulin. The results obtained supported our assumption that full-length Nup358 is enriched in the nuclear fraction whereas the shorter form is present in the cytoplasm (Fig. 6A). As a spliced transcript encoding Nup358 has not been reported, the mechanism of producing the short form of Nup358, in neurons, remains poorly understood. However, it is tempting to speculate that there is a developmental switch in expression of Nup358 isoforms by which the shorter form concentrates at the AIS in mature neurons.

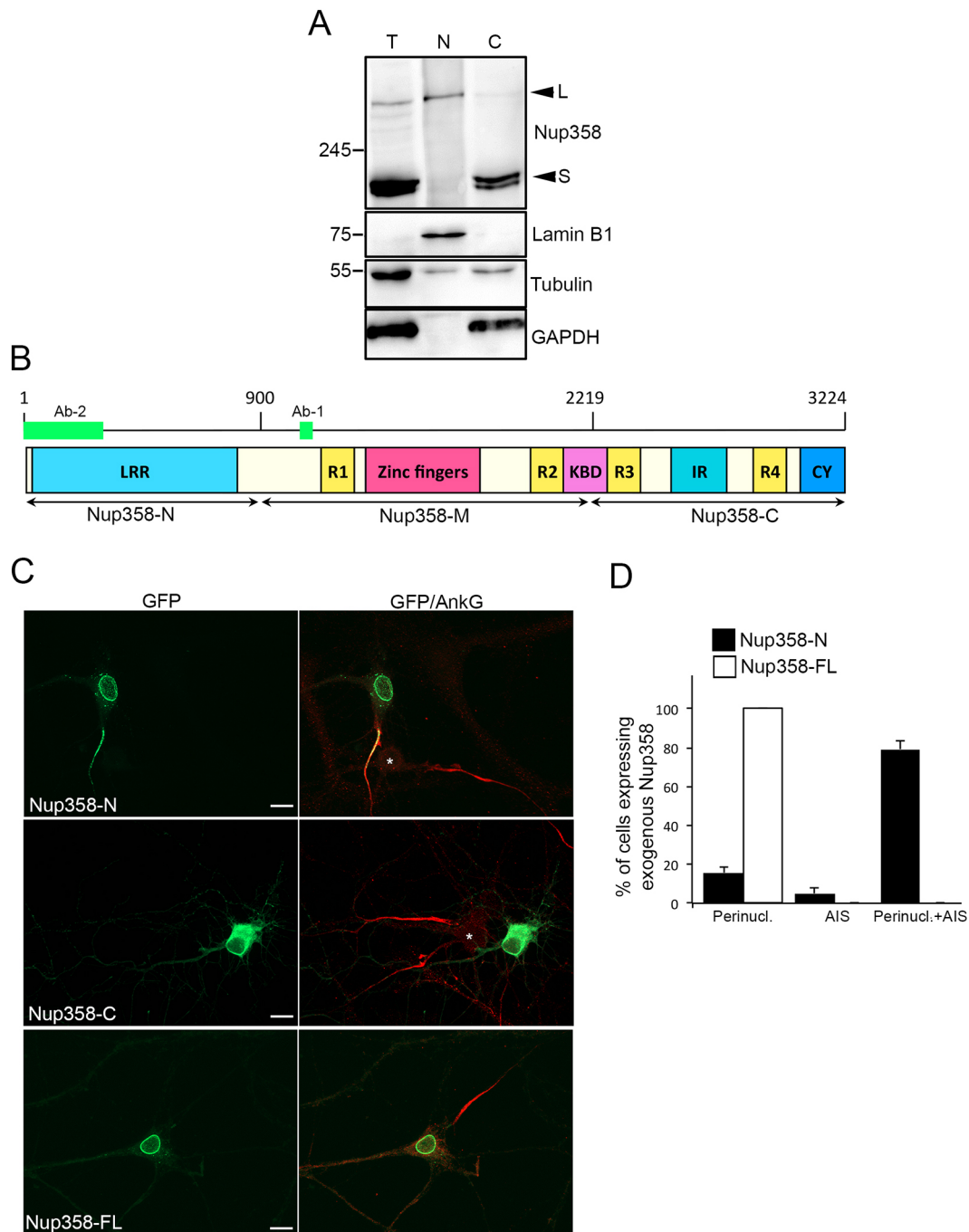


**Fig. 6. The N-terminus of Nup358 is the region crucial for its targeting to the AIS.** (A) Immunoblot of Nup358 from total lysate (T), nuclear-enriched (N) and cytoplasm-enriched (C) fractions of 14 DIV neuronal lysate. Immunoblotting for lamin B1 (nuclear marker),  $\beta$ -tubulin and GAPDH were done to validate the efficiency of the fractionation. (B) Schematic representation of human Nup358 composed of 3224 amino acid residues and showing its different domains: leucine-rich region (LRR), four RanGTP-binding domains (R1–R4), kinesin-binding domain (KBD), internal repeats (IR), and cyclophilin A homology domain (CY). The regions Ab-1 and Ab-2 are the recognition sites of the anti-Nup358 antibodies used in this study. Also shown are the regions expressed by the constructs used in transfections: the N-terminal region (Nup358-N; residues 1–900), the middle region (Nup358-M; residues 901–2219), and the C-terminal region (Nup358-C; residues 2220–3224). (C) Immunofluorescence images of rat hippocampal neurons transfected with the constructs GFP–Nup358-N, GFP–Nup358-C and GFP–Nup358-FL. 13 DIV rat hippocampal neurons were transfected with the corresponding construct, maintained afterward in culture for 48 h, then fixed and immunostained for AnkG to identify the axon initial segment. Asterisks are used to mark neighboring non-transfected neurons. Scale bars: 10  $\mu$ m. (D) Analysis of the percentage of neurons expressing exogenous Nup358-N and Nup358-FL at the perinuclear region and/or the AIS. The results shown are mean  $\pm$  s.e.m. of three independent experiments, with  $n=35$  (Nup358-N) and  $n=21$  (Nup358-FL).

### The N-terminal region of Nup358 is crucial for its association with the AIS

Nup358 protein includes multiple motifs that interact selectively with cellular proteins depending on the cell type and its physiological state

(Aslanukov et al., 2006; Cai et al., 2001; Cho et al., 2007; Joseph and Dasso, 2008; Lin et al., 2013; Sahoo et al., 2017; Singh et al., 1999; Wu et al., 1995). We therefore aimed to identify the region of Nup358 responsible for its association with the AIS, and possibly represents



the site of interaction with other AIS proteins. For this purpose, fusions of GFP to different fragments of Nup358 (Fig. 6B) were expressed in neurons and examined for their localization pattern. Preliminary experiments were performed in HeLa cells to verify the expression of the constructs. The N-terminal region of Nup358 (GFP–Nup358-N) was expressed as filamentous structures surrounding the cell nucleus (Fig. S6A, Nup358-N), presumably attached to microtubules as previously reported (Joseph and Dasso, 2008). The middle and C-terminal regions of Nup358 (GFP–Nup358-M and GFP–Nup358-C) both showed a more diffuse pattern, yet in distinct subcellular locations. GFP–Nup358-M was preferentially present inside the nucleus, whereas GFP–Nup358-C was found in the cytoplasm of HeLa cells (Fig. S6A, Nup358-M and Nup358-C). Finally, full-length Nup358 (GFP–Nup358-FL) localized in the perinuclear region and in the cytoplasm (Fig. S6A, Nup358-FL), overlapping with endogenous Nup358. Since the endogenous puncta of Nup358 associate with the ER (see Fig. 2A), we assessed whether exogenous Nup358-N also colocalizes with ER staining. HeLa cells were transfected with mCherry–Nup358-N then fixed and immunostained for Sec61A, an ER membrane protein. However, Sec61A seemed to be wrapping around the mCherry–Nup358-N signal in the cytoplasm of HeLa cells (Fig. S6B). We assume that when Nup358-N is overexpressed in HeLa cells, its subcellular localization is shifted towards the cytoskeleton, particularly to the microtubules, which regulate ER distribution and movement in the cell (Gurel et al., 2014).

In a neuronal context, GFP–Nup358-N was expressed at the nuclear rim, in the cell soma and the AIS (Fig. 6C, Nup358-N), in a pattern very similar to that of endogenous Nup358. This result, therefore, suggests that the N-terminus of Nup358 includes the region crucial for its association with the NPC (Joseph and Dasso, 2008) (see Fig. 6C) and its recruitment to the AIS (see Fig. 6C). Expression of GFP–Nup358-M was not detected in neurons, whereas GFP–Nup358-C had a diffuse pattern in the cytoplasm of neuronal cells (Fig. 6C, Nup358-C). Surprisingly, GFP–Nup358-FL was expressed exclusively at the perinuclear region with no marked signal at the AIS (Fig. 6C, Nup358-FL).

To examine the possible relocation of GFP–Nup358-FL to the AIS, we prolonged the culture period post-transfection to 96 h; however, the distribution profile did not change (data not shown). Quantitatively, we confirmed the differential localization of exogenous Nup358 (or its mutant) in transfected neurons. The majority of GFP–Nup358-N-transfected neurons exhibited a signal at both the AIS and the perinuclear region, and a small population of neurons expressed Nup358-N in one region but not the other (Fig. 6D, Nup358-N). In contrast, all of the neurons transfected with GFP–Nup358-FL displayed signal only at the nuclear rim (Fig. 6D, Nup358-FL). This difference in subcellular localization of GFP–Nup358-N and GFP–Nup358-FL might be related to the presence of two isoforms of Nup358 (see Fig. 5A,C, Fig. 6A).

Next, we sought to downregulate Nup358 using shRNA constructs and rescue its phenotype by exogenous expression of full-length Nup358 or its N-terminal region. Neurons at 6 DIV were co-transfected with GFP–sh-Nup358, and either mCherry–Nup358-FL or mCherry–Nup358-N. Three days post-transfection, neurons were fixed and examined for their expression of the exogenous protein. Given that transfecting primary neurons with a construct as big as mCherry–Nup358-FL (~14 kb) is generally challenging, none of the cells were successfully co-transfected with both constructs. However, a few neurons were co-transfected with GFP–sh-Nup358 and mCherry–Nup358-N that was expressed around cell nuclei and at the AIS (data not shown), therefore

supporting our assumption that the N-terminus of Nup358 is essential for its association with the AIS.

Because of their considerable large size, GFP or mCherry might influence the subcellular localization of exogenous Nup358. Thus, in neurons, we transiently expressed fusions of Nup358 fragments to a smaller-sized epitope tag, V5. Mouse cortical neurons at 7 DIV were transfected with V5–Nup358-N or V5–Nup358-FL, fixed after 48 h in culture, and immunostained for Sec61A. Results were comparatively similar to the constructs tagged with GFP and mCherry, showing V5–Nup358-N at both the perinuclear and the AIS, while V5–Nup358-FL localized exclusively at the nuclear rim (Fig. S6C). Subsequently, we tested whether the presence of V5 at the N-terminus of Nup358 influences its subcellular localization. Cultured neurons were transfected with constructs having V5 at the C-terminal end of the Nup358 constructs. Although transfection efficiency was markedly low, Nup358-N–V5 was either detected in the perinuclear region or at the AIS but not in both regions of the same transfected neuron. Nup358-FL–V5 was only detected at the nuclear rim of transfected neurons (data not shown). Of note, when HeLa cells were transfected with the Nup358-N–V5 construct, exogenous Nup358 was abundantly expressed as aggregates in the cytoplasm, as well as around cell nuclei (data not shown), suggesting possible interference of a C-terminal V5 tag with the folding of exogenous Nup358.

Despite the N-terminal fragment being present in both Nup358-FL and Nup358-N, these constructs varied in their subcellular distribution, possibly owing to the presence of the two isoforms of Nup358 (see Fig. 5A, Nup358-S and Nup358-L). Full-length Nup358 is exclusively present in the perinuclear region (see Fig. 6A, Nup358-L) while the shorter form of Nup358 is observed in the cytoplasm (see Fig. 6A, Nup358-S).

### Stimulating neurons with pharmacological drugs reduces the expression of Nup358

Because of a high concentration of voltage-gated sodium ( $\text{Na}_v$ ) channels, the AIS is a highly excitable neuronal subdomain that is responsible for synaptic input integration and action potential generation (Leterrier, 2018). Accumulating evidence has shown that during short- or long-term changes in neuronal activity, the AIS is dynamically modulated by changes in its structural and functional characteristics (Grubb and Burrone, 2010a; Grubb et al., 2011; Kuba et al., 2015; Muir and Kittler, 2014). To assess whether inhibiting or stimulating neuronal activity with specific drugs would alter Nup358 expression and subcellular distribution, 14 DIV neurons were treated with: (1) tetrodotoxin (TTX), which blocks  $\text{Na}_v$  channels, thereby inhibiting action potentials; (2) bicuculline (BIC), which blocks the inhibitory function of  $\text{GABA}_A$  receptors, thus indirectly stimulating neurons; (3) 4-AP, which blocks voltage-gated  $\text{K}^+$  channels and consequently prolongs the duration of action potentials, and (4) BIC and 4-AP simultaneously. Afterwards, neurons were fixed and immunostained for Nup358 and AnkG (Fig. 7). Nup358 subcellular distribution was almost the same in treated and control neurons, but with a marked decrease in its signal intensity in some of the treatments applied (data not shown). We quantified the total fluorescence intensity of Nup358 within neuronal cells. Inhibiting neuronal activity with TTX had no effect on Nup358 signal intensity (Fig. 7A, TTX); however, when neurons were stimulated with 4-AP alone or in combination with BIC, Nup358 total fluorescence intensity was significantly reduced by  $15 \pm 1.21\%$  (Fig. 7A, 4-AP) and by  $27 \pm 2.03\%$  (mean  $\pm$  s.e.m.) (Fig. 7A, BIC+4-AP) as a result of the synergistic effect of these drugs. Next, we analyzed in greater detail whether these reductions

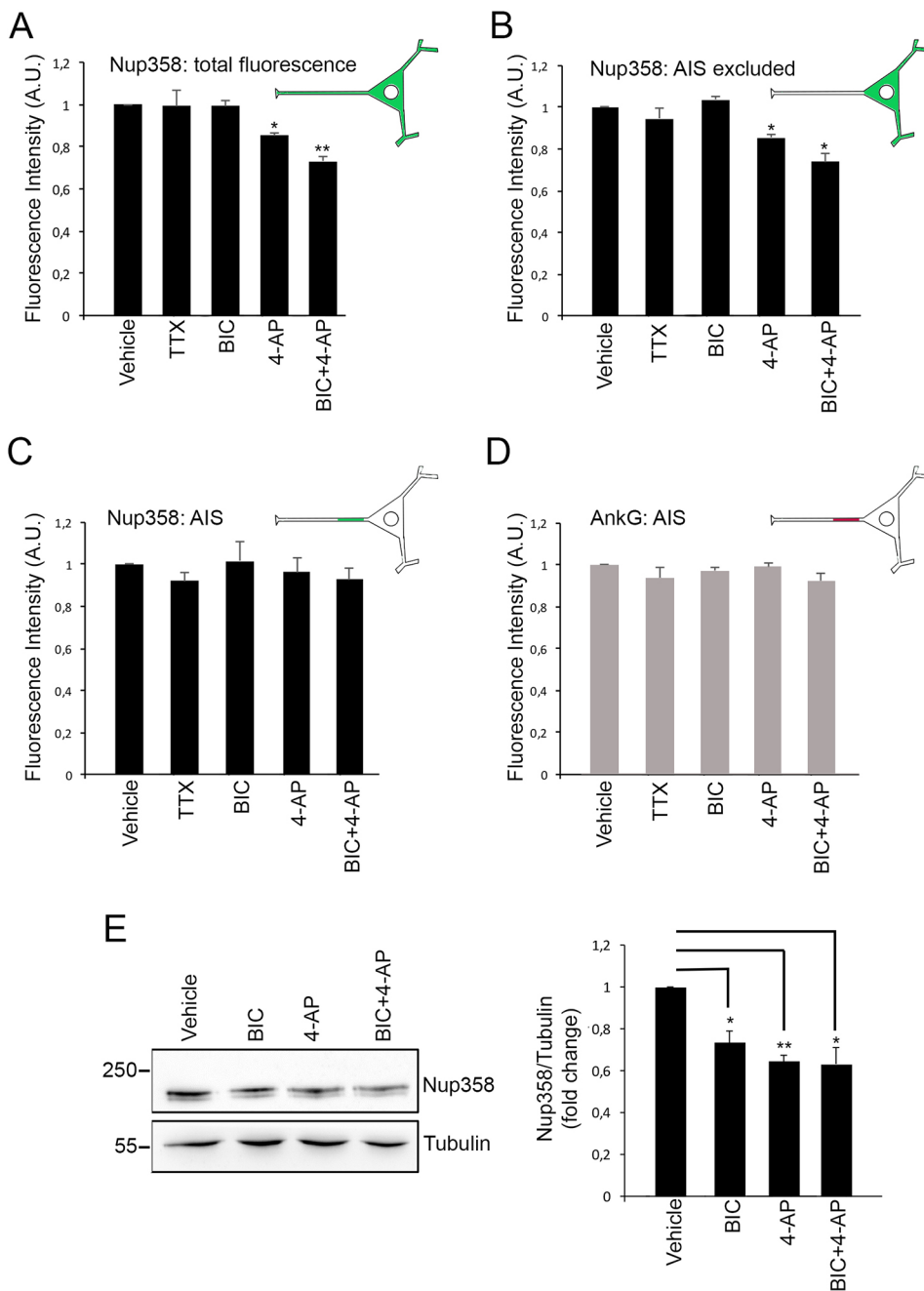


**Fig. 7. Nup358 expression is reduced following neuronal stimulation.** 14 DIV cortical neurons were treated overnight with DMSO (vehicle) as control, tetrodotoxin (TTX; 1  $\mu$ M), bicuculline (BIC; 50  $\mu$ M) and/or 4-aminopyridine (4-AP; 0.5 mM). (A–D) High-content analysis of Nup358 and AnkG fluorescence intensities. Nup358 or AnkG mean fluorescence intensity in neurons ( $n > 2000$ ) is quantified and normalized to the mean intensity in vehicle-treated neurons, therefore the results represent relative fluorescence intensity in arbitrary units (A.U.). Alongside each histogram, a schematic drawing of the neuronal cell demonstrating the region selected for the analysis (colored in green or red). (A) Nup358 fluorescence intensity is measured in entire neuronal cells and depicted as ‘Nup358: total fluorescence’ with statistical analysis as follows: vehicle to TTX,  $P = 0.747$ ; vehicle to BIC,  $P = 0.683$ ; vehicle to 4-AP,  $P = 0.029$ ; vehicle to BIC+4-AP,  $P = 0.001$ . (B) Nup358 fluorescence intensity is measured in the neuronal cells but excluding Nup358 pool at the AIS, thus denoted as ‘Nup358: AIS excluded’ with statistical analysis as follows: vehicle to TTX,  $P = 0.342$ ; vehicle to BIC,  $P = 0.96$ ; vehicle to 4-AP,  $P = 0.022$ ; vehicle to BIC+4-AP,  $P = 0.01$ . (C) Nup358 fluorescence intensity is measured at the level of the AIS, thus denoted as ‘Nup358: AIS’; all treatments with  $P > 0.05$ . (D) AnkG fluorescence intensity is indicated as ‘AnkG: AIS’; all treatments with  $P > 0.05$ . (E) Immunoblot of the short form of Nup358 from neuronal lysates treated with BIC and/or 4-AP, alongside band intensity quantification relative to tubulin. Data obtained from statistical analysis are as follows: vehicle to BIC,  $P = 0.044$ ; vehicle to 4-AP,  $P = 0.007$ ; vehicle to BIC+4-AP,  $P = 0.043$ . The results presented are mean  $\pm$  s.e.m. of three independent experiments. \* $P < 0.05$  and \*\* $P < 0.01$  (one-way ANOVA followed by Dunnett’s post hoc test).

in Nup358 signal hail from the AIS or the somatodendritic compartment. We measured Nup358 signal at the AIS based on its overlap with AnkG staining, thus termed ‘Nup358: AIS’; and the remaining signal of Nup358 in the neuronal cell, mostly at the nuclear rim and soma, was termed ‘Nup358: AIS excluded’. The resulting analysis showed that with 4-AP or BIC+4-AP, Nup358 intensity in the somatodendritic domain significantly dropped by  $15 \pm 1.72\%$  and  $26 \pm 3.94\%$ , respectively, in a manner that mirrored the decrease in the total fluorescence intensity of Nup358 (Fig. 7B, and see Fig. 7A). At the AIS, there was no change in Nup358 or AnkG fluorescence intensity upon any of the treatments (Fig. 7C,D). Under the same experimental conditions, we analyzed Nup358 protein expression using western blotting (Fig. 7E). The analysis was conducted on the short isoform of Nup358 as it is the predominant form in 14 DIV neurons, with  $\beta$ -tubulin serving as a

loading control. The results were comparable with the analyses of Nup358 fluorescence intensity (see Fig. 7A,B), showing a significant decrease in Nup358 protein expression upon the treatment with BIC, 4-AP, or with both simultaneously (Fig. 7E). Taken together, these data show that stimulating neurons reduces the overall expression levels of Nup358 without interfering with the Nup358 pool at the AIS.

#### KCl treatment decreases Nup358 expression

After demonstrating that increasing neuronal activity alters Nup358 protein expression, we wondered whether depolarizing neurons with KCl, a commonly used treatment for stimulating neurons, would have a similar effect on Nup358. In parallel, control neurons were treated with an equivalent concentration of NaCl to maintain the osmotic concentration of monovalent ions. In KCl-treated

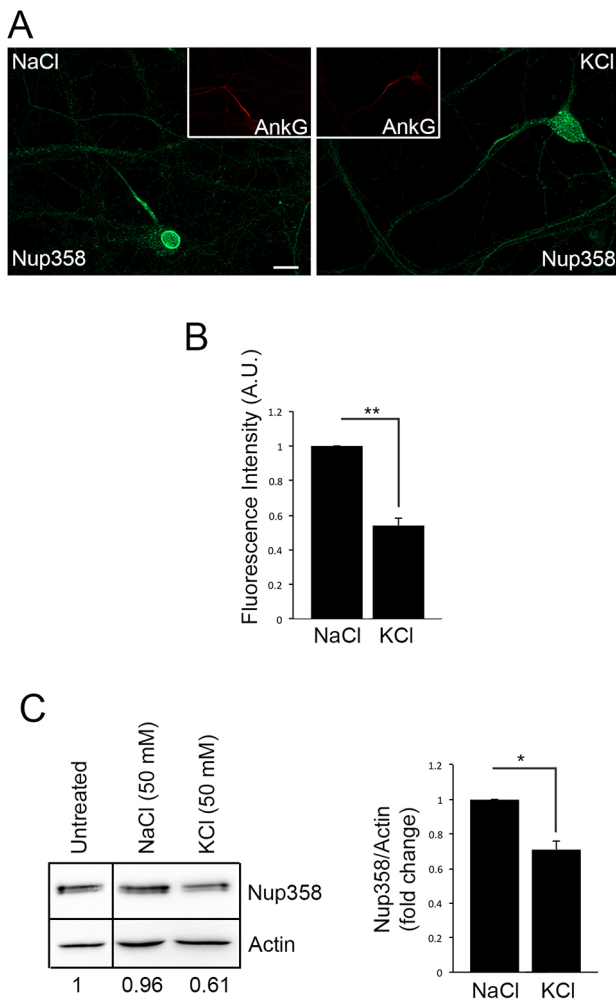


**Fig. 8. Treating neurons with KCl triggers a decrease in Nup358 expression.** (A) Immunofluorescence images of Nup358 and AnkG in 14 DIV neurons treated with either KCl (50 mM, 1 h) or an equivalent concentration of NaCl as a control. Scale bar: 10  $\mu$ m. (B) Quantitative analysis of Nup358 fluorescence intensity in NaCl- versus KCl-treated neurons ( $n > 2000$  and  $P = 0.007$ ). Arbitrary units, A.U. (C) Immunoblot for the short form of Nup358 and actin in NaCl- and KCl-treated neuronal lysates with the graph showing the corresponding quantification of Nup358:actin ratio ( $P = 0.015$ ). The results expressed are mean  $\pm$  s.e.m. of three independent experiments. \* $P < 0.05$  and \*\* $P < 0.01$  (two-tailed Student's *t*-test).

neurons, Nup358 subcellular distribution was notably altered, with a decrease in its signal at the nuclear rim and a more diffuse staining in the entire neuronal cell, whereas at the AIS, Nup358 signal was noticeably persistent (Fig. 8A). Quantitative analysis of Nup358 total fluorescence intensity showed a gross reduction of  $46 \pm 4.32\%$  (mean  $\pm$  s.e.m.) in KCl-treated neurons (Fig. 8B), that was further reflected in a decrease in its protein expression level (Fig. 8C). Because membrane depolarization with KCl increases calcium influx through voltage-gated calcium channels or NMDA and/or AMPA receptors (La Montanara et al., 2015), we assessed their involvement in the KCl-mediated effect on Nup358. Neurons were pretreated with EGTA to block calcium entry, APV to block NMDA receptors (NMDARs) or CNQX to block AMPA receptors. Using the Operetta high-content imaging system, we analyzed Nup358 fluorescence intensity in the entire neuronal cell (Nup358: total fluorescence), and the subcellular regions (Nup358: AIS excluded and Nup358: AIS), in addition to measuring AnkG signal (AnkG:

AIS). Compared to the control (NaCl-treated), KCl-treated neurons exhibited reduced levels in Nup358 mean fluorescence intensity (Fig. S7A, KCl) and an equivalent decrease in Nup358 signal in the subcellular regions including the AIS (Fig. S7B,C, KCl). In contrast to BIC and 4-AP (see Fig. 7B,C), KCl treatment induces a partial disassembly of the AIS where Nup358 and AnkG signals are reduced (Fig. S7B,C, KCl) (Letierrier et al., 2015). This KCl-mediated effect was alleviated when neurons were pretreated with either EGTA or APV but not with CNQX (Fig. S7A–C). Likewise, western blotting analysis of Nup358 expression showed partial to complete recovery when neurons were pretreated with EGTA and APV, respectively, and no recovery at all when neurons were pretreated with CNQX (Fig. S8A).

These results prove that treating neurons with KCl imposes an excitotoxic insult, resulting in NMDAR activation and elevated calcium influx. The downstream calcium-dependent proteolytic enzymes known as calpains would then be activated (Adamec et al., 1998; Andres et al., 2013) and ultimately cleave substrates of receptors, enzymes or cytoskeletal proteins (Chan and Mattson, 1999), and possibly Nup358. In support of this notion, previous reports have shown that in diverse excitotoxic events, nucleoporins such as Nup153, Nup62, Nup88 and Nup358 were cleaved by activated calpains (Bano et al., 2010; Sugiyama et al., 2017; Yamashita et al., 2017). Moreover, under conditions of an increased calcium concentration, calpains contribute to the proteolysis of such AIS proteins as AnkG (Letierrier et al., 2015). Thus, to assess this hypothesis, neurons were pretreated with the calpain inhibitor ALLM (25  $\mu$ M) for 30 min (Wu et al., 2004), then with KCl. Calpain activation was evaluated through the degradation of  $\beta$ II-spectrin (260 kDa) into stable breakdown products including a 110 kDa fragment (Kobeissy et al., 2015). Compared to the control, KCl-treated neurons exhibited a strong signal from the 110 kDa breakdown product of  $\beta$ II-spectrin, and this effect was ameliorated when ALLM was included in the treatment (Fig. S8B). The pretreatment with ALLM resulted in a moderate recovery in Nup358-S protein level but not Nup358-L. These findings prove that an acute treatment of neurons with KCl affects Nup358 protein level in neurons through a mechanism involving overactivation of NMDA receptors, subsequent calcium influx, and ultimately calpain activation.

## DISCUSSION

Nup358 (RanBP2) was first identified as a giant nucleoporin present at the cytoplasmic side of the nuclear pore complex (Yokoyama et al., 1995). This description has evolved over the past decades as Nup358 was detected in regions other than the perinuclear and shown to be involved in a myriad of physiological events (Aslanukov et al., 2006; Cai et al., 2001; Cho et al., 2007; Hashizume et al., 2013; Joseph et al., 2004; Vyas et al., 2013). In neurons, Nup358 is involved in axon specification by interacting with the Par polarity complex proteins, dishevelled and aPKC (Vyas et al., 2013). However, the comprehensive mechanism that underlines the role of Nup358 in developing and mature neurons is poorly investigated. Here, we demonstrate that a pool of Nup358 associates, remarkably, with the axon initial segment (AIS) of mature neurons, mediated by the scaffolding protein AnkG. Because the AIS is a unique neuronal region that maintains neuronal polarity and represents the spike initiation zone (Rasband, 2010; Yoshimura and Rasband, 2014), our data thus suggest that Nup358 has a non-classical but a specialized role in neuronal cells.

AnkG is one of the early markers detected at the AIS and it serves as a key scaffold for clustering other AIS proteins (Jenkins and Bennett, 2001; Pan et al., 2006; Rasmussen et al., 2007; Sánchez-

Ponce et al., 2012; Zhou et al., 1998). Consistent with these studies, AnkG was identified early during neuronal development and prior to Nup358 expression at this region. AnkG induces Nup358 to associate with the AIS whereas Nup358 is crucial for the long-term stability of AnkG; when Nup358 was downregulated, AnkG signal was dramatically reduced. Such an interdependent relationship between AnkG and other AIS proteins has only previously been observed with the membranous proteins Na<sub>v</sub> channels and NF-186. Upon knockdown of AnkG membrane partners, Na<sub>v</sub> channels or NF-186, AnkG expression was significantly reduced, therefore compromising the formation and maintenance of the AIS (Leterrier et al., 2017). This phenotype was rescued when the ankyrin-binding domain of Na<sub>v</sub>1.2 and an anchor to the plasma membrane were exogenously expressed (Leterrier et al., 2017). Nup358, however, does not have a transmembrane domain that would similarly influence AnkG association with the AIS. Nevertheless, in our neuronal cultures, a few neurons, particularly at late developmental stages, exhibited a distinct submembranous localization of Nup358. One possible scenario is that Nup358 protein includes a yet-undefined ankyrin- or membrane-binding domain that facilitates its association with the plasma membrane. Alternatively, Nup358 might undergo post-translational modifications that modulate its recruitment to the AIS. Above all, whether Nup358 interacts directly with AnkG requires further investigation since both proteins colocalize at the AIS of cultured neurons and in the inner plexiform layer of the mouse retina as well. Furthermore, both AnkG and neurofascin were identified together with immunoprecipitated Nup358. This finding further supports our assumptions of an interaction between Nup358 and AIS proteins. The axon initial segment and nodes of Ranvier (NOR) share almost the same molecular composition: the scaffold protein AnkG, Na<sub>v</sub> channels, the cytoskeletal protein βIV-spectrin (also known as Sptbn4) and the cell adhesion molecule NF-186 (Nelson and Jenkins, 2017). Nup358 was found to be expressed at NOR and extended to the paranodes flanking NOR, where contactin, contactin-associated protein (CASPR), and glial neurofascin NF-155 are present (Nelson and Jenkins, 2017). Therefore, depending on its interaction with different partner proteins, Nup358 might serve different functions at the AIS and the paranodes. In a previous study, Nup358 was shown to regulate axon specification in developing neurons by binding to dishevelled and aPKC proteins (Vyas et al., 2013). With our data showing Nup358 being expressed at the AIS and having an interdependent relationship with AnkG, we suggest that Nup358 interacts with AIS proteins and maintains their long-term stability in this region. Without Nup358, AnkG expression at the AIS will be reduced, thus resulting in a disassembly of the AIS protein composition, and compromising neuronal polarity and proper cellular function.

Another important finding of this study is the detection of two isoforms of Nup358 that were differentially expressed during neuronal development. Nup358 has previously been detected at its high molecular mass, 358 kDa in humans (Bernad et al., 2004; Wu et al., 1995; Yokoyama et al., 1995). Here, Nup358 is expressed as two isoforms, one full-length, detected at increasing levels as neurons develop, and a shorter form, detected at levels that decrease conversely to the full-length form. These isoforms also differ in their subcellular distribution. The shorter form is predominant in the cytoplasm and is probably the isoform associated with the AIS, whereas full-length Nup358 is detected in the nuclear fraction. Although a spliced variant of Nup358 has not been reported, one possible scenario for this differential expression would involve a developmental switch by which the shorter isoform is predominant

in mature neurons. To identify the region of Nup358 that selectively associates with the AIS, we exogenously expressed different fragments of Nup358 and monitored their subcellular localization. Our results show that the N-terminal region is sufficient for localization at the AIS and the perinuclear region, but despite this, full-length Nup358 includes the N-terminal region yet exhibits a different distribution pattern. We assume that the full-length isoform includes an amino acid sequence restricting its localization to the nuclear envelope. In contrast, the shorter isoform perhaps lacks this sequence and thus has a more dynamic behavior and is capable of accumulation at the AIS.

What is the mechanism that dictates Nup358 targeting to the AIS? In our cultures of cortical neurons, a fraction of the Nup358 total pool localizes at the endoplasmic reticulum. Nup358 association with the ER might serve as a reservoir for Nup358 to be recruited to the AIS. In support of this hypothesis, the cytoplasmic fraction of neuronal lysate, which includes the pools of Nup358 at the ER and the AIS, contains only the short isoform of Nup358. The Nup358 pool at the ER might have an alternative role acting as a chaperone for specific proteins. For instance, Nup358 interacts with the red and green opsins and modulates their subcellular localization in photoreceptors (Ferreira et al., 1996). Our finding of Nup358 at the ER, however, contradicts a previous report identifying Nup358 with other nucleoporins at the annulate lamellae (AL) of neurons (Raghunayakula et al., 2015), which are membranous organelles with characteristic features of both the endoplasmic reticulum and NPCs. Our data show that AL are scarce in neurons and nucleoporins are predominantly expressed at the nuclear rim associated with NPCs. Nup358, instead, has a unique subcellular distribution, being present at the perinuclear region, ER and the AIS, therefore suggesting a specialized role of Nup358 in neurons. For instance, Cho et al. (2017) showed that conditional ablation of Nup358 in mouse motoneurons results in various traits that resemble amyotrophic lateral sclerosis-like syndrome such as hypoactivity, hindlimb paralysis and decreased nerve conduction velocity. We thus propose that these effects are partly attributed to the fact that Nup358 associates with both the AIS and NOR.

The AIS is characterized by structural and functional plasticity modulated by neuronal excitability (Yamada and Kuba, 2016). However, we show that when stimulating neurons with 4-AP alone or in combination with BIC, there was an overall decrease in Nup358 expression with no significant change at the level of the AIS. Although Nup358 might be more stable at the AIS than in other regions of the neuronal cell, we cannot exclude the possibility that an increase in neuronal activity would result in changes in Nup358 expression with respect to changes in AIS length and its position along the axon as previous studies have reported morphological plasticity of the AIS (Leterrier, 2018). Further studies in a more homogenous population of neuronal cells, such as hippocampal culture, would provide a better understanding of Nup358 modulation at the AIS.

In conclusion, while Nup358 is conventionally associated with NPCs, it exhibits a unique distribution profile in neurons: one fraction of the total pool is present at the nuclear envelope associated with NPCs, another fraction colocalizes with the ER, and a third fraction accumulates at the AIS, dependent on the key AIS protein AnkG. Future studies, however, are required to better examine the dynamics of Nup358 distribution profile and identify the function of Nup358 at the AIS.

## MATERIALS AND METHODS

### Antibodies

Primary antibodies employed in immunofluorescence (IF) and western blotting (WB): two closely related rabbit anti-Nup358 against a region

between amino acids 1050–1100 of Nup358 (IF 1:100; WB 1:2000; Abcam ab197044; Bethyl A301-796A), mouse anti-Nup358 against amino acids 1–300 of the N-terminus (WB 1:2000; Santa Cruz Biotechnology sc-74518), mouse anti-Nup88 (IF 1:100, WB 1:2000; Santa Cruz Biotechnology sc-136009), mouse anti-Nup98 (IF 1:100, WB 1:2000; Santa Cruz Biotechnology sc-74578), mouse anti-m414 (IF 1:100; Abcam ab50008), mouse anti-AnkG (IF 1:100; Neuromab 75-146; Invitrogen 33-8800), mouse anti-MAP2 (IF 1:500; Sigma-Aldrich M4403), mouse anti- $\beta$ III-tubulin (IF 1:300; Sigma-Aldrich T8578), mouse anti-Golgi P58 (IF 1:100; Sigma-Aldrich C2404), mouse anti-COX1 (IF 1:100; Abcam ab14705), mouse anti-calnexin (IF 1:100; Abcam ab31290), chicken anti-neurofascin (IF 1:500; Invitrogen PA5-47468), mouse anti-CASPR (IF 1:200; Neuromab 75-001), mouse anti-actin (WB 1:4000; Abcam ab3280), mouse anti-Nup153 (WB 1:2000; Abcam ab24700), mouse anti-GAPDH (WB 1:4000; Santa Cruz Biotechnology sc-32233), rabbit anti- $\beta$ -tubulin (WB 1:4000; Cell Signaling Technology 2128), and goat anti-lamin B1 (WB 1:2000; Santa Cruz Biotechnology sc-30264). The corresponding secondary antibodies used for immunofluorescence were goat anti-rabbit Alexa Fluor 488-conjugated (1:800; Invitrogen A11008), goat anti-rabbit Alexa Fluor 594-conjugated (1:800; Invitrogen A11012), goat anti-mouse Alexa Fluor 594-conjugated (1:800; Invitrogen A11020), and goat anti-mouse Alexa Fluor 647-conjugated (1:200; Abcam ab150115). For western blotting, the following horseradish peroxidase (HRP)-conjugated secondary antibodies were used (all are 1:5000; Santa Cruz Biotechnology): goat anti-mouse, goat anti-rabbit and donkey anti-goat.

### Constructs

The plasmids used for the knockdown experiments were: scrambled negative control shRNA (sh-CTRL, Origene TR30021), and a pool of four mouse gene-specific Nup358 shRNA constructs (sh-Nup358, Origene TL501860) in pGFP-C-shLenti Vector (Origene). The sh-AnkG target sequence, AGT TCA GAG GAA GTG AGT TAC, was retrieved from the RNAi Consortium (TRC) mouse shRNA library (<https://www.broadinstitute.org/mai-consortium/mai-consortium-shrna-library>) and the oligonucleotides were designed according to the TRC guidelines. The annealed oligonucleotides were then cloned into a pLKO.1 vector modified by swapping the puromycin resistance gene with an EGFP expression cassette. For the transient expression of green fluorescent protein (GFP)-Nup358 or its different fragments, the following constructs were kindly provided by Prof. Jomon Joseph (Joseph and Dasso, 2008): full-length Nup358 (GFP-Nup358-FL; amino acids 1–3224), N-terminal region (GFP-Nup358-N; amino acids 1–900), middle-region (GFP-Nup358-M; amino acids 901–2219), and the C-terminal region (GFP-Nup358-C; amino acids 2220–3224). The other Nup358 plasmids coexpressing V5 or mCherry were constructed by replacing the GFP in the GFP-Nup358-N and GFP-Nup358-FL plasmids with V5 or mCherry using standard cloning techniques.

### Animals

Animal care and experimental procedures were conducted in accordance with the University of Trento ethics committee and were approved by the Italian Ministry of Health.

### Cell culture

Cortical and hippocampal cultures were prepared from E15 and E17 mouse embryos, respectively, using a previously described method (Qian et al., 1998; Pischedda et al., 2018) with some modifications. Briefly, cortices or hippocampi were dissected from C57BL/6 mouse brains and treated with papain solution [papain (20 U, Worthington), EDTA (5 mM), and cysteine (30 mM) in 1 $\times$  Earle's balanced salt solution (EBSS, Gibco)] for about 20 min in a 37°C water bath, with occasional swirling of the mixture. Complete dissociation of neuronal cells was achieved mechanically, using gentle trituration through a serological pipette. DNase I (1 mg/ml, Sigma-Aldrich) was added to the neuron suspension and incubated for 3 min at 37°C. Next, the cells were pelleted at 1000 $\times$  g for 5 min, resuspended in an EBSS solution supplemented with bovine serum albumin (10 mg/ml, Sigma-Aldrich) and trypsin inhibitor (10 mg/ml, Sigma-Aldrich), and centrifuged again at 1000 $\times$  g for 10 min. The pellet obtained was resuspended in minimal essential medium with Glutamax (Gibco)

supplemented with 10% fetal bovine serum (FBS) and plated on poly-D-lysine-coated substrates (10  $\mu$ g/ml, Sigma-Aldrich). Cells were allowed to attach to the substrate in a humidified 37°C, 5% CO<sub>2</sub> incubator for 24 h, after which half the volume of the culture medium was replaced by neurobasal medium (Invitrogen) supplemented with 2% B-27 (Invitrogen) and AraC (5  $\mu$ M, Sigma-Aldrich). Cultures were maintained up to 21 days *in vitro* (DIV), during which one half of the culture medium was replenished with fresh growth medium at 7 and 14 DIV. Rat hippocampal cultures were prepared according to a previously described protocol (Goetze et al., 2006). HeLa cells (ATCC) were grown in DMEM (Gibco) supplemented with 10% FBS (Gibco) and 1% penicillin/streptomycin.

### Transfections

HeLa cells were transfected with Nup358 constructs using Viafect reagent (Promega) according to the manufacturer's instructions. Protein expression was allowed to proceed for 2 days at 37°C in a humidified 5% CO<sub>2</sub> incubator. Mouse cortical neurons were transfected with shRNA constructs using Lipofectamine LTX or Lipofectamine Plus reagent (Invitrogen) according to the manufacturer's instructions with a few modifications. In brief, 5 DIV cultured neurons were subjected to a medium change; the old medium was collected and kept equilibrated in the 5% CO<sub>2</sub> incubator for later use. Transfections were allowed to proceed for 2 h, after which the medium was replaced with one-half volume of fresh growth medium and another half of the old medium. Transfected neurons were maintained in culture for 5 days, then fixed with 4% PFA and processed for immunofluorescence. Using the same protocol, 6 DIV mouse cortical neurons were transfected with V5-Nup358 (or Nup358-V5) expression plasmids and maintained in culture for 3 days. For the transient expression of GFP-Nup358-FL, GFP-Nup358-N, GFP-Nup358-M and GFP-Nup358-C in neurons, we used the calcium phosphate protocol instead (Goetze et al., 2004) to transfect 13 DIV rat hippocampal neurons, which were then maintained in culture for 2–4 days before being fixed and immunostained. To quantify Nup358 downregulation through western blotting analysis, lentiviruses were produced by transient transfection of HEK293T cells according to standard protocols (Wiznerowicz and Trono, 2003). Primary cortical cultures were transduced at DIV 4 with lentiviruses at multiplicity of infection 3 (MOI 3).

### Treatments

To test whether inhibiting transcription affects the distribution profile of Nup358, neurons were treated with either actinomycin D (ActD; 5  $\mu$ g/ml) or DMSO (vehicle) as a control for 1 h along with 5-ethynyl uridine (EU; 0.5 mM, Thermo Fisher Scientific) which is a uracil analog that gets incorporated into nascent RNA during transcription. As for the detergent extraction experiments, cultured cortical neurons were washed briefly with a pre-warmed HBSS, then incubated with 1% Triton X-100 in the cytoskeletal buffer (2 mM MgCl<sub>2</sub>, 1 mM EGTA, 60 mM PIPES buffer pH 7.0) for 5 min at 37°C (Winckler et al., 1999). In some cases, neurons were extracted for 24 min at 37°C during which the Triton solution was replenished every 8 min. Afterward, neurons were washed and processed for immunostaining. Nup358 association with the neuronal cytoskeleton was examined by perturbing actin filaments or microtubules. To depolymerize actin filaments, neurons were treated with cytochalasin D (CytoD; 10  $\mu$ M, Sigma-Aldrich) for 1 h whereas to disrupt microtubules, neurons were treated with nocodazole (Noc; 20  $\mu$ M, Sigma-Aldrich) for 3 h and as a negative control, neurons were incubated with DMSO alone (vehicle). To address the influence of neuronal activity on Nup358 protein expression and distribution profile, the following treatments were conducted overnight: tetrodotoxin (TTX; 1  $\mu$ M, Sigma-Aldrich), bicuculline (BIC; 50  $\mu$ M, Sigma-Aldrich), 4-aminopyridine (4-AP; 500  $\mu$ M, Sigma-Aldrich), and in some cases, neurons were co-treated with BIC and 4-AP simultaneously. Treatment of neurons with KCl was carried out for 1 h by adding KCl to a final concentration of 50 mM in complete neurobasal medium. Wherever mentioned, the KCl-treatment was preceded by a 30 min incubation with any of: EGTA (2 mM), APV (100  $\mu$ M, Sigma-Aldrich), CNQX (40  $\mu$ M, Santa Cruz Biotechnology), or ALLM (25  $\mu$ M, Santa Cruz Biotechnology). Following these treatments, neurons were fixed and processed for immunocytochemistry; otherwise, neurons were immediately lysed and prepared for western blotting. All these treatments were conducted on 14 DIV cortical neurons.

### Immunostaining

Cultured neurons were washed with pre-warmed HBSS and fixed with 4% PFA for 15 min at room temperature. Cells were then rinsed three times with PBS, 5 min each, and immunofluorescence was carried out as follows: neurons were permeabilized with 0.1% Triton X-100 in PBS for 10 min, then incubated with the blocking solution (2% BSA, 2% FBS, 0.2% gelatin in PBS) for 1 h at room temperature. Incubation with primary antibodies was done overnight at 4°C, subsequently, incubation with the respective Alexa Fluor-conjugated secondary antibodies was carried out for 1 h at room temperature. For the detection of actin filaments, neurons were incubated with Alexa Fluor 594 phalloidin (1:50; Invitrogen A12381) for 20 min at room temperature (Goetze et al., 2004). Nuclei were stained with DAPI for 10 min after which coverslips were mounted using Mowiol and allowed to dry overnight at 4°C. 5-EU (5-ethynyl uridine) labeling was detected with a click chemical reaction. After fixation and blocking, neurons were incubated for 30 min with 10 μM 5-FAM-azide fluorescent label (5-FAM, Jena Bioscience) in the following solution (100 mM Tris pH 8.5, 1 mM CuSO<sub>4</sub>, 100 mM ascorbic acid). Subsequently, neurons were washed three times in TBS buffer–0.5% Triton X-100, followed by immunostaining for Nup358 as described above. For immunohistochemistry, 15-μm-thick retinal and 20-μm-thick sciatic nerve sections were prepared from an adult mouse samples using standard protocols. Slides with cryosections were thawed and allowed to dry at room temperature. The retinal sections were washed for 5 min in PBS buffer and incubated for 1 h at room temperature in blocking solution (PBS containing 10% FBS, 1% BSA and 0.5% Triton X-100). Sections were incubated with primary antibodies against Nup358 and AnkG (1:100) in a diluted blocking solution (3% FBS, 1% BSA, 0.5% Triton X-100 in PBS); incubation was conducted overnight at 4°C, then antibodies were replenished through addition of a fresh primary antibody solution for another overnight incubation. Next, the sections were washed three times with PBS, 15 min each, and incubated with secondary antibodies for 2 h at room temperature in the diluted blocking solution, then washed again three times with PBS. A few drops of Mowiol were added on each section, and a coverslip was carefully placed on the top. Alternatively, the sciatic nerve sections were permeabilized for 45 min with PBS-T (0.3% Triton X-100) then blocked for 1 h in 5% BSA-PBS-T. Primary antibodies against Nup358 and neurofascin (1:500) or CASPR (1:200) were diluted in the blocking solution and incubated overnight at 4°C. Next, the sections were washed three times for 10 min with PBS-T, and incubated with anti-rabbit Cy3 (1:1000; Dianova 111-165-003) and anti-chicken Alexa Fluor 647 (1:1000; Invitrogen A21449) secondary antibodies for 1 h at room temperature. After incubation, the sections were washed three times for 10 min and incubated for 5 min with DAPI, then washed again and mounted with ProLong diamond mounting medium (Invitrogen).

### Imaging

Microscopy analysis was performed using the 63× oil objective of a Zeiss Observer Z.1 microscope, equipped with an ApoTome.2 module. Images were acquired and processed into orthogonal projections of 15–0 optical z-planes (0.24 μm interval), using ZEN 2 imaging software (Zeiss). Confocal images of retinal tissue sections were acquired using a Leica TCS SP5 confocal microscope while images of the sciatic nerve sections were acquired using Leica TCS SP8 and Olympus IX81 confocal microscopes. All images were assembled using Adobe Photoshop CS6.

### Colocalization and fluorescence intensity analysis

For colocalization analysis, double-labeled images of 15 optical sections were analyzed using Fiji-ImageJ. Background subtraction was performed using a constant value of the rolling ball radius. Regions of interest (ROI) such as the AIS or the Golgi were selected using the lasso tool and traced around the area to be analyzed. For less confined staining in cells, such as in the ER and mitochondria, ROIs were selected using 3D objects counter. To evaluate colocalization between Nup358 and the different subcellular markers, Manders' coefficients ranging from 0 to 1 were quantified using Coloc2 plugin. Positive colocalization was recognized when above-threshold values of Manders' coefficient were  $\geq 0.6$ . To ensure reliable analysis of colocalization, single-labeled images were used as negative controls and

examined for bleed-through where they showed no signal in the opposite channel. To measure the fluorescence intensity of Nup358 and Ank-G at the level of the AIS in Nup358- and AnkG-downregulated neurons, we acquired images and analyzed them using ImageJ software. A ROI was traced around the AIS in GFP-positive and in GFP-negative cells. Fluorescence intensity is expressed as mean intensity (MI) reported in GFP-positive cells over MI measured in untransfected cells present in the same field.

### High-content analysis

Cortical neurons (60,000 cells/well) were plated in 96-well Cell Carrier plates (PerkinElmer) and allowed to grow to 14 DIV, the day on which drug treatments were conducted. To maximize the accuracy of the analysis, each condition was conducted in five replicate wells. Neurons were fixed and immunolabeled for Nup358 and AnkG as described previously. Images were acquired using the 40× objective of an Operetta high-content imaging system (PerkinElmer) where at least 18 fields were selected per well. Analysis of Nup358 fluorescence intensity was conducted using Columbus 2.2 software (PerkinElmer). Neuronal cells were identified based on DAPI staining of their nuclei, and segmentation of the neuronal network was achieved by applying a combination of algorithmic parameters. This segmentation, therefore, allowed for a comprehensive analysis of Nup358 fluorescence intensity at the level of the AIS (marked by AnkG staining) and the somatodendritic compartment and neuronal processes excluding the AIS, in addition to a total intensity value (Nup358 fluorescence in the entire neuronal cell). All measurements were corrected by subtracting the background intensity and they represent mean fluorescence intensities.

### Western blotting

To analyze changes in Nup358 protein expression during neuronal development, cultured neurons were collected at different DIV. Cells were washed briefly with ice-cold PBS, then scraped and lysed in CHAPS lysis buffer [0.5% CHAPS (Sigma-Aldrich), 1 μM EDTA, 150 μM NaCl, 50 μM Tris-HCl pH 7.4, 10% glycerol, and protease inhibitor cocktail (Roche)]. Cortex, hippocampus and spinal cord samples were isolated from mice at embryonic day (E18) and during the postnatal period (P3–P90), and then homogenized using the same CHAPS lysis buffer. Homogenization was conducted using a motor-driven Dounce homogenizer (Heidolph) to apply 10–15 strokes at 1000 rpm in a glass tissue grinder. Cell lysates or crude tissue homogenates were then centrifuged at 10,600× *g* for 10 min at 4°C. The supernatant of each sample was collected, and equal amounts of protein were loaded on a 5–8% gradient SDS-PAGE gel. Prior to protein transfer onto a nitrocellulose membrane (GE Healthcare Sciences), the SDS-PAGE gel was rinsed for 2 min in the fixing solution (40% methanol, 10% acetic acid, 50% Milli-Q water). The transfer was carried out overnight at 4°C, at low voltage (40 V), and immunoblotting was performed according to standard protocols. For the nucleocytoplasmic fractionation experiment, neurons were lysed with STEN lysis buffer (STEN buffer: 50 mM Tris pH 7.6, 150 mM NaCl, 2 mM EDTA, 0.2% Nonidet P-40. STEN lysis buffer: 1% Triton X-100, 1% Nonidet P-40, Roche protease inhibitor cocktail, in STEN buffer) to isolate the cytoplasmic-enriched fraction (Benvegnù et al., 2017), and the nuclear-enriched fraction was collected with RIPA buffer (Thermo Scientific 89901) according to the protocol. The total lysate sample of 14 DIV cortical neurons was obtained using CHAPS buffer as above. In all buffers, protease inhibitor cocktail was included.

### Immunoprecipitation

Immunoprecipitation of Nup358 was performed using homogenates of P30 mouse cortices. 2 μg of rabbit polyclonal anti-Nup358, designated Ab-1 in the main text (see Fig. 6B), was added to 500 μl of the tissue homogenate overnight at 4°C, while 2 μg of rabbit anti-IgG antibody (Millipore 12-370) was used instead for the control sample. 30 μl of Dynabeads Protein A magnetic beads (Invitrogen) were washed once with ice-cold CHAPS lysis buffer and incubated with the immunocomplex solution at room temperature for 30 min. Beads were then washed three times and processed for western blotting.

### Coomassie Blue staining and mass-spectrometric analysis

After gel electrophoresis, staining was conducted for 30 min at room temperature using rapid Coomassie Blue stain (Melford) diluted in 5% acetic acid, 7.5% methanol solution. To destain the gel, repeated washings were done with the 5% acetic acid, 7.5% methanol solution until the bands became visible. Relative to the protein ladder, the 230 kDa band of Nup358 was identified in the Nup358 immunoprecipitated sample, cut with a sterile scalpel and analyzed by mass spectrometry (Proteomic Unit, Cogentech).

### Statistical analysis

All experiments were carried out in triplicate, unless mentioned otherwise, with independent mouse dissections. Immunofluorescence images are representative images of at least three independent experiments. Results, shown as mean±s.e.m., were evaluated using SPSS with the following statistical tests: two-tailed Student's *t*-test (for two groups) and one-way ANOVA with Dunnett's post hoc (for control against other groups) where *P*<0.05 was considered statistically significant.

### Acknowledgements

We thank Prof. Jomon Joseph (National Center for Cell Science, Pune University, India) for kindly providing the plasmids to express full-length as well as deleted GFP-tagged Nup358, and we thank Prof. Simona Casarosa (Department of Cellular, Computational and Integrative Biology—CIBIO, University of Trento, Italy) and Dr Xuwen Zhang (Department of Cellular, Computational and Integrative Biology—CIBIO, University of Trento, Italy) for the retinal cryosections. We acknowledge Dr Valentina Adami and Michael Pancher (CIBIO High Throughput Screening Core Facility, University of Trento, Italy) for their technical assistance. Thanks also go to Dr Michela Rocuzzo and Dr Sara Leo (CIBIO Advanced Imaging Core Facility, University of Trento, Italy) for their excellent support during image acquisition and colocalization analyses. And we thank Prof. Dr Artuhr Mayerhofer (BMC-Cell Biology, Munich, Germany) for helping with the sciatic nerve dissection, Dr Steffen Dietzel (Core Facility Bioimaging BMC-Munich, Germany) for the excellent support during image acquisition of sections, and the Protein Analysis Unit of BMC-Munich (Germany) for their help with the mass spectrometry analysis. We are grateful to Dr Marie-Laure Baudet (Department of Cellular, Computational and Integrative Biology—CIBIO, University of Trento, Italy) for the critical comments on the manuscript. We also thank Dr Jovica Ninkovic (Department for Cell Biology BioMedizinisches Centrum, Munich, Germany) for the CASPR staining and for the imaging of the sciatic nerve sections.

### Competing interests

The authors declare no competing or financial interests.

### Author contributions

Conceptualization: B.K., M.K., P.M.; Methodology: B.K., A.R., F.P., A.C., S.T., M.K.; Validation: B.K., F.P.; Formal analysis: B.K., F.P., G.P.; Investigation: B.K.; Resources: A.R., A.C., M.K.; Data curation: B.K., F.P., G.P.; Writing - original draft: B.K., P.M.; Writing - review & editing: B.K., F.P., S.T., G.P., M.K., P.M.; Supervision: S.T., G.P., M.K., P.M.; Project administration: P.M.; Funding acquisition: P.M.

### Funding

This work was supported by the University of Trento (Progetto Biotecnologie).

### Supplementary information

Supplementary information available online at <http://jcs.biologists.org/lookup/doi/10.1242/jcs.222802.supplemental>

### References

- Adamec, E., Beermann, M. L., Nixon, R. A. (1998). Calpain I activation in rat hippocampal neurons in culture is NMDA receptor selective and not essential for excitotoxic cell death. *Brain Res. Mol. Brain Res.* **54**, 35-48. doi:10.1016/s0169-328x(97)00304-5
- Andres, A. L., Regev, L., Phi, L., Seese, R. R., Chen, Y., Gall, C. M. and Baram, T. Z. (2013). NMDA receptor activation and calpain contribute to disruption of dendritic spines by the stress neuropeptide CRH. *J. Neurosci.* **33**, 16945-16960. doi:10.1523/JNEUROSCI.1445-13.2013
- Aslanukov, A., Bhowmick, R., Guraju, M., Oswald, J., Raz, D., Bush, R. A., Sieving, P. A., Lu, X., Bock, C. B. and Ferreira, P. A. (2006). RanBP2 modulates Cox11 and hexokinase I activities and haploinsufficiency of RanBP2 causes deficits in glucose metabolism. *PLoS Genet.* **2**, e177. doi:10.1371/journal.pgen.0020177
- Bano, D., Dinsdale, D., Cabrera-Socorro, A., Maida, S., Lambacher, N., McColl, B., Ferrando-May, E., Hengartner, M. O. and Nicotera, P. (2010). Alteration of

- the nuclear pore complex in Ca<sup>2+</sup>-mediated cell death. *Cell Death Differ.* **17**, 119-133. doi:10.1038/cdd.2009.112
- Benvegnù, S., Mateo, M. I., Palomer, E., Jurado-Arjona, J. and Dotti, C. G. (2017). Aging triggers cytoplasmic depletion and nuclear translocation of the E3 ligase mahogunin: a function for ubiquitin in neuronal survival. *Mol. Cell* **66**, 358-372.e7. doi:10.1016/j.molcel.2017.04.005
- Bernad, R., van der Velde, H., Fornerod, M. and Pickersgill, H. (2004). Nup358/RanBP2 attaches to the nuclear pore complex via association with Nup88 and Nup214/CAN and plays a supporting role in CRM1-mediated nuclear protein export. *Mol. Cell. Biol.* **24**, 2373-2384. doi:10.1128/MCB.24.6.2373-2384.2004
- Bodoor, K., Shaikh, S., Salina, D., Raharjo, W. H., Bastos, R., Lohka, M. and Burke, B. (1999). Sequential recruitment of NPC proteins to the nuclear periphery at the end of mitosis. *J. Cell Sci.* **112**, 2253-2264.
- Cai, Y., Singh, B. B., Aslanukov, A., Zhao, H. and Ferreira, P. A. (2001). The docking of kinesins, KIF5B and KIF5C, to Ran-binding protein 2 (RanBP2) is mediated via a novel RanBP2 domain. *J. Biol. Chem.* **276**, 41594-41602. doi:10.1074/jbc.M104514200
- Chan, S. L. and Mattson, M. P. (1999). Caspase and calpain substrates: roles in synaptic plasticity and cell death. *J. Neurosci. Res.* **58**, 167-190. doi:10.1002/(SICI)1097-4547(19991001)58:1<167::AID-JNR16>3.0.CO;2-K
- Chatel, G. and Fahrenkrog, B. (2012). Dynamics and diverse functions of nuclear pore complex proteins. *Nucleus* **3**, 162-171. doi:10.4161/nucl.19674
- Chatel, G., Desai, S. H., Mattheyses, A. L., Powers, M. A. and Fahrenkrog, B. (2012). Domain topology of nucleoporin Nup98 cein the nuclear pore complex. *J. Struct. Biol.* **177**, 81-89. doi:10.1016/j.jsb.2011.11.004
- Cho, K.-I., Cai, Y., Yi, H., Yeh, A., Aslanukov, A. and Ferreira, P. A. (2007). Association of the kinesin-binding domain of RanBP2 to KIF5B and KIF5C determines mitochondria localization and function. *Traffic* **8**, 1722-1735. doi:10.1111/j.1600-0854.2007.00647.x
- Cho, K.-I., Yoon, D., Qiu, S., Danziger, Z., Grill, W. M., Wetsel, W. C. and Ferreira, P. A. (2017). Loss of Ranbp2 in motoneurons causes disruption of nucleocytoplasmic and chemokine signaling, proteostasis of hnRNPH3 and Mmp28, and development of amyotrophic lateral sclerosis-like syndromes. *Dis. Model. Mech.* **10**, 559-579. doi:10.1242/dmm.027730
- Cordes, V. C., Reidenbach, S. and Franke, W. W. (1996). Cytoplasmic annulate lamellae in cultured cells: composition, distribution, and mitotic behavior. *Cell Tissue Res.* **284**, 177-191. doi:10.1007/s004410050578
- Cronshaw, J. M., Krutchinsky, A. N., Zhang, W., Chait, B. T. and Matunis, M. J. (2002). Proteomic analysis of the mammalian nuclear pore complex. *J. Cell Biol.* **158**, 915-927. doi:10.1083/jcb.200206106
- D'Angelo, M. A. and Hetzer, M. W. (2006). The role of the nuclear envelope in cellular organization. *Cell. Mol. Life Sci.* **63**, 316-332. doi:10.1007/s00018-005-5361-3
- D'Angelo, M. A., Gomez-Cavazos, J. S., Mei, A., Lackner, D. H. and Hetzer, M. W. (2012). A change in nuclear pore complex composition regulates cell differentiation. *Dev. Cell* **22**, 446-458. doi:10.1016/j.devcel.2011.11.021
- Davis, L. I. and Blobel, G. (1986). Identification and characterization of a nuclear pore complex protein. *Cell* **45**, 699-709. doi:10.1016/0092-8674(86)90784-1
- Dawlaty, M. M., Malureanu, L., Jeganathan, K. B., Kao, E., Sustmann, C., Tahk, S., Shuai, K., Grosschedl, R. and van Deursen, J. M. (2008). Resolution of sister centromeres requires RanBP2-mediated SUMOylation of topoisomerase I $\alpha$ . *Cell* **133**, 103-115. doi:10.1016/j.cell.2008.01.045
- Delphin, C., Guan, T., Melchior, F. and Gerace, L. (1997). RanGTP targets p97 to RanBP2, a filamentous protein localized at the cytoplasmic periphery of the nuclear pore complex. *Mol. Biol. Cell* **8**, 2379-2390. doi:10.1091/mbc.8.12.2379
- Dennerlein, S. and Rehling, P. (2015). Human mitochondrial COX1 assembly into cytochrome c oxidase at a glance. *J. Cell Sci.* **128**, 833-837. doi:10.1242/jcs.161729
- Einheber, S., Zanazzi, G., Ching, W., Scherer, S., Milner, T. A., Peles, E. and Salzer, J. L. (1997). The axonal membrane protein Caspr, a homologue of neuexin IV, is a component of the septate-like paranodal junctions that assemble during myelination. *J. Cell Biol.* **139**, 1495-1506. doi:10.1083/jcb.139.6.1495
- Ferreira, P. A., Nakayama, T. A., Pak, W. L. and Travis, G. H. (1996). Cyclophilin-related protein RanBP2 acts as chaperone for red/green opsin. *Nature* **383**, 637-640. doi:10.1038/383637a0
- Fornerod, M., van Deursen, J., van Baal, S., Reynolds, A., Davis, D., Murti, K. G., Fransen, J. and Grosveld, G. (1997). The human homologue of yeast CRM1 is in a dynamic subcomplex with CAN/Nup214 and a novel nuclear pore component Nup88. *EMBO J.* **16**, 807-816. doi:10.1093/emboj/16.4.807
- Galiano, M. R., Jha, S., Ho, T. S.-Y., Zhang, C., Ogawa, Y., Chang, K.-J., Stankewich, M. C., Mohler, P. J. and Rasband, M. N. (2012). A distal axonal cytoskeleton forms an intra-axonal boundary that controls axon initial segment assembly. *Cell* **149**, 1125-1139. doi:10.1016/j.cell.2012.03.039
- Goetze, B., Grunewald, B., Baldassa, S. and Kiebler, M. (2004). Chemically controlled formation of a DNA/calcium phosphate coprecipitate: application for transfection of mature hippocampal neurons. *J. Neurobiol.* **60**, 517-525. doi:10.1002/neu.20073
- Goetze, B., Tuebing, F., Xie, Y., Dorostkar, M. M., Thomas, S., Pehl, U., Boehm, S., Macchi, P. and Kiebler, M. A. (2006). The brain-specific double-stranded

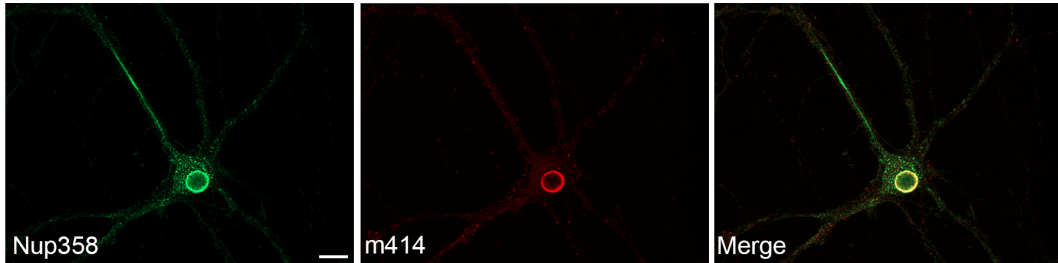
- RNA-binding protein Staufen2 is required for dendritic spine morphogenesis. *J. Cell Biol.* **172**, 221-231. doi:10.1083/jcb.200509035
- Griffis, E. R., Altan, N., Lippincott-Schwartz, J. and Powers, M. A.** (2002). Nup98 is a mobile nucleoporin with transcription-dependent dynamics. *Mol. Biol. Cell* **13**, 1282-1297. doi:10.1091/mbc.01-11-0538
- Griffis, E. R., Craige, B., Dimaano, C., Ullman, K. S. and Powers, M. A.** (2004). Distinct functional domains in nucleoporins Nup153 and Nup98 mediate transcription-dependent mobility. *Mol. Biol. Cell* **15**, 1991-2002. doi:10.1091/mbc.e03-10-0743
- Grubb, M. S. and Burrone, J.** (2010a). Activity-dependent relocation of the axon initial segment fine-tunes neuronal excitability. *Nature* **465**, 1070-1074. doi:10.1038/nature09160
- Grubb, M. S. and Burrone, J.** (2010b). Building and maintaining the axon initial segment. *Curr. Opin. Neurobiol.* **20**, 481-488. doi:10.1016/j.conb.2010.04.012
- Grubb, M. S., Shu, Y., Kuba, H., Rasband, M. N., Wimmer, V. C. and Bender, K. J.** (2011). Short- and long-term plasticity at the axon initial segment. *J. Neurosci.* **31**, 16049-16055. doi:10.1523/JNEUROSCI.4064-11.2011
- Guan, T., Kehlenbach, R. H., Schirmer, E. C., Kehlenbach, A., Fan, F., Clurman, B. E., Arnheim, N. and Gerace, L.** (2000). Nup50, a nucleoplasmically oriented nucleoporin with a role in nuclear protein export. *Mol. Cell. Biol.* **20**, 5619-5630. doi:10.1128/MCB.20.15.5619-5630.2000
- Gurel, P. S., Hatch, A. L. and Higgs, H. N.** (2014). Connecting the cytoskeleton to the endoplasmic reticulum and Golgi. *Curr. Biol.* **24**, R660-R672. doi:10.1016/j.cub.2014.05.033
- Hashizume, C., Kobayashi, A. and Wong, R. W.** (2013). Down-modulation of nucleoporin RanBP2/Nup358 impaired chromosomal alignment and induced mitotic catastrophe. *Cell Death Dis.* **4**, e854. doi:10.1038/cddis.2013.370
- Hedstrom, K. L., Xu, X., Ogawa, Y., Frischknecht, R., Seidenbecher, C. I., Shrago, P. and Rasband, M. N.** (2007). Neurofascin assembles a specialized extracellular matrix at the axon initial segment. *J. Cell Biol.* **178**, 875-886. doi:10.1083/jcb.200705119
- Hedstrom, K. L., Ogawa, Y. and Rasband, M. N.** (2008). AnkyrinG is required for maintenance of the axon initial segment and neuronal polarity. *J. Cell Biol.* **183**, 635-640. doi:10.1083/jcb.200806112
- Jenkins, S. M. and Bennett, V.** (2001). Ankyrin-G coordinates assembly of the spectrin-based membrane skeleton, voltage-gated sodium channels, and L1 CAMs at Purkinje neuron initial segments. *J. Cell Biol.* **155**, 739-746. doi:10.1083/jcb.200109026
- Joseph, J. and Dasso, M.** (2008). The nucleoporin Nup358 associates with and regulates interphase microtubules. *FEBS Lett.* **582**, 190-196. doi:10.1016/j.febslet.2007.11.087
- Joseph, J., Liu, S.-T., Jablonski, S. A., Yen, T. J. and Dasso, M.** (2004). The RanGAP1-RanBP2 complex is essential for microtubule-kinetochore interactions in vivo. *Curr. Biol.* **14**, 611-617. doi:10.1016/j.cub.2004.03.031
- Kessel, R. G.** (1992). Annulate lamellae: a last frontier in cellular organelles. *Int. Rev. Cytol.* **133**, 43-120. doi:10.1016/S0074-7696(08)61858-6
- Kobeissy, F. H., Liu, M. C., Yang, Z., Zhang, Z., Zheng, W., Glushakova, O., Mondello, S., Anagli, J., Hayes, R. L. and Wang, K. K. W.** (2015). Degradation of  $\beta$ -II-Spectrin Protein by Calpain-2 and Caspase-3 Under Neurotoxic and Traumatic Brain Injury Conditions. *Mol. Neurobiol.* **52**, 696-709. doi:10.1007/s12035-014-8898-z
- Krull, S., Thyberg, J., Björkroth, B., Rackwitz, H.-R. and Cordes, V. C.** (2004). Nucleoporins as components of the nuclear pore complex core structure and Tpr as the architectural element of the nuclear basket. *Mol. Biol. Cell* **15**, 4261-4277. doi:10.1091/mbc.e04-03-0165
- Kuba, H., Yamada, R., Ishiguro, G. and Adachi, R.** (2015). Redistribution of Kv1 and Kv7 enhances neuronal excitability during structural axon initial segment plasticity. *Nat. Commun.* **6**, 8815. doi:10.1038/ncomms9815
- La Montanara, P., Rusconi, L., Locarno, A., Forti, L., Barbiero, I., Tramarin, M., Chandola, C., Kilstrup-Nielsen, C. and Landsberger, N.** (2015). Synaptic synthesis, dephosphorylation, and degradation: a novel paradigm for an activity-dependent neuronal control of CDKL5. *J. Biol. Chem.* **290**, 4512-4527. doi:10.1074/jbc.M114.589762
- Leterrier, C.** (2018). The axon initial segment: an updated viewpoint. *J. Neurosci.* **38**, 2135-2145. doi:10.1523/JNEUROSCI.1922-17.2018
- Leterrier, C. and Dargent, B.** (2014). No Pasaran! Role of the axon initial segment in the regulation of protein transport and the maintenance of axonal identity. *Semin. Cell Dev. Biol.* **27**, 44-51. doi:10.1016/j.semcdb.2013.11.001
- Leterrier, C., Potier, J., Caillol, G., Debarnot, C., Rueda Boroni, F. and Dargent, B.** (2015). Nanoscale architecture of the axon initial segment reveals an organized and robust scaffold. *Cell Rep.* **13**, 2781-2793. doi:10.1016/j.celrep.2015.11.051
- Leterrier, C., Clerc, N., Rueda-Boroni, F., Montersino, A., Dargent, B. and Castets, F.** (2017). Ankyrin G membrane partners drive the establishment and maintenance of the axon initial segment. *Front. Cell. Neurosci.* **11**, 6. doi:10.3389/fncel.2017.00006
- Lin, D. H., Zimmermann, S., Stuwe, T., Stuwe, E. and Hoelz, A.** (2013). Structural and functional analysis of the C-terminal domain of Nup358/RanBP2. *J. Mol. Biol.* **425**, 1318-1329. doi:10.1016/j.jmb.2013.01.021
- Lupu, F., Alves, A., Anderson, K., Doye, V. and Lacy, E.** (2008). Nuclear pore composition regulates neural stem/progenitor cell differentiation in the mouse embryo. *Dev. Cell* **14**, 831-842. doi:10.1016/j.devcel.2008.03.011
- Mahajan, R., Delphin, C., Guan, T., Gerace, L. and Melchior, F.** (1997). A small ubiquitin-related polypeptide involved in targeting RanGAP1 to nuclear pore complex protein RanBP2. *Cell* **88**, 97-107. doi:10.1016/S0092-8674(00)81862-0
- Mavlyutov, T. A., Cai, Y. and Ferreira, P. A.** (2002). Identification of RanBP2- and kinesin-mediated transport pathways with restricted neuronal and subcellular localization. *Traffic* **3**, 630-640. doi:10.1034/j.1600-0854.2002.30905.x
- Miller, B. R. and Forbes, D. J.** (2000). Purification of the vertebrate nuclear pore complex by biochemical criteria. *Traffic* **1**, 941-951. doi:10.1034/j.1600-0854.2000.011204.x
- Muir, J. and Kittler, J. T.** (2014). Plasticity of GABAA receptor diffusion dynamics at the axon initial segment. *Front. Cell. Neurosci.* **8**, 151. doi:10.3389/fncel.2014.00151
- Nelson, A. D. and Jenkins, P. M.** (2017). Axonal membranes and their domains: assembly and function of the axon initial segment and node of Ranvier. *Front. Cell. Neurosci.* **11**, 136. doi:10.3389/fncel.2017.00136
- Pan, Z., Kao, T., Horvath, Z., Lemos, J., Sul, J.-Y., Cranston, S. D., Bennett, V., Scherer, S. S. and Cooper, E. C.** (2006). A common ankyrin-G-based mechanism retains KCNQ and NaV channels at electrically active domains of the axon. *J. Neurosci.* **26**, 2599-2613. doi:10.1523/JNEUROSCI.4314-05.2006
- Patil, H., Yoon, D., Bhowmick, R., Cai, Y., Cho, K.-I. and Ferreira, P. A.** (2017). Impairments in age-dependent ubiquitin proteostasis and structural integrity of selective neurons by uncoupling Ran GTPase from the Ran-binding domain 3 of Ranbp2 and identification of novel mitochondrial isoforms of ubiquitin-conjugating enzyme E21 (ubc9) and Ranbp2. *Small GTPases* **10**, 146-161. doi:10.1080/21541248.2017.1356432
- Pischedda, F., Montani, C., Obergasteiger, J., Frapporti, G., Corti, C., Rosato Siri, M., Volta, M. and Piccoli, G.** (2018). Cryopreservation of primary mouse neurons: the benefit of neurostore cryoprotective medium. *Front. Cell. Neurosci.* **12**, 81. doi:10.3389/fncel.2018.00081
- Qian, X., Goderie, S. K., Shen, Q., Stern, J. H. and Temple, S.** (1998). Intrinsic programs of patterned cell lineages in isolated vertebrate CNS ventricular zone cells. *Development* **125**, 3143-3152.
- Rabut, G., Doye, V. and Ellenberg, J.** (2004). Mapping the dynamic organization of the nuclear pore complex inside single living cells. *Nat. Cell Biol.* **6**, 1114-1121. doi:10.1038/ncb1184
- Raghuayakula, S., Subramonian, D., Dasso, M., Kumar, R. and Zhang, X.-D.** (2015). Molecular characterization and functional analysis of annulate lamellae pore complexes in nuclear transport in mammalian cells. *PLoS ONE* **10**, e0144508. doi:10.1371/journal.pone.0144508
- Rasband, M. N.** (2010). The axon initial segment and the maintenance of neuronal polarity. *Nat. Rev. Neurosci.* **11**, 552-562. doi:10.1038/nrn2852
- Rasmussen, H. B., Frøkjær-Jensen, C., Jensen, C. S., Jensen, H. S., Jørgensen, N. K., Misonou, H., Trimmer, J. S., Olesen, S.-P. and Schmitt, N.** (2007). Requirement of subunit co-assembly and ankyrin-G for M-channel localization at the axon initial segment. *J. Cell Sci.* **120**, 953-963. doi:10.1242/jcs.03396
- Reichelt, R., Holzenburg, A., Buhle, E. L., Jarnik, M., Engel, A. and Aebi, U.** (1990). Correlation between structure and mass distribution of the nuclear pore complex and of distinct pore complex components. *J. Cell Biol.* **110**, 883-894. doi:10.1083/jcb.110.4.883
- Sahoo, M. R., Gaikwad, S., Khuperkar, D., Ashok, M., Helen, M., Yadav, S. K., Singh, A., Magre, I., Deshmukh, P., Dhanvijay, S. et al.** (2017). Nup358 binds to AGO proteins through its SUMO-interacting motifs and promotes the association of target mRNA with miRISC. *EMBO Rep.* **18**, 241-263. doi:10.15252/embr.201642386
- Salina, D., Enarson, P., Rattner, J. B. and Burke, B.** (2003). Nup358 integrates nuclear envelope breakdown with kinetochore assembly. *J. Cell Biol.* **162**, 991-1001. doi:10.1083/jcb.200304080
- Sánchez-Ponce, D., DeFelipe, J., Garrido, J. J. and Muñoz, A.** (2012). Developmental expression of Kv potassium channels at the axon initial segment of cultured hippocampal neurons. *PLoS ONE* **7**, e48557. doi:10.1371/journal.pone.0048557
- Saraste, J., Palade, G. E., Farquhar, M. G.** (1987). Antibodies to rat pancreas Golgi subfractions: identification of a 58-kD cis-Golgi protein. *J. Cell Biol.* **105**, 2021-2029. doi:10.1083/jcb.105.5.2021
- Sherman, D. L., Tait, S., Melrose, S., Johnson, R., Zonta, B., Court, F. A., Macklin, W. B., Meek, S., Smith, A. J. H., Cottrell, D. F. et al.** (2005). Neurofascins are required to establish axonal domains for saltatory conduction. *Neuron* **48**, 737-742. doi:10.1016/j.neuron.2005.10.019
- Singh, B. B., Patel, H. H., Roepman, R., Schick, D. and Ferreira, P. A.** (1999). The zinc finger cluster domain of RanBP2 is a specific docking site for the nuclear export factor, exportin-1. *J. Biol. Chem.* **274**, 37370-37378. doi:10.1074/jbc.274.52.37370
- Sugiyama, K., Aida, T., Nomura, M., Takayanagi, R., Zeilhofer, H. U. and Tanaka, K.** (2017). Calpain-dependent degradation of nucleoporins contributes to motor neuron death in a mouse model of chronic excitotoxicity. *J. Neurosci.* **37**, 8830-8844. doi:10.1523/JNEUROSCI.0730-17.2017
- Sukegawa, J. and Blobel, G.** (1993). A nuclear pore complex protein that contains zinc finger motifs, binds DNA, and faces the nucleoplasm. *Cell* **72**, 29-38. doi:10.1016/0092-8674(93)90047-T
- Suntharalingam, M. and Wente, S. R.** (2003). Peering through the pore: nuclear pore complex structure, assembly, and function. *Dev. Cell* **4**, 775-789. doi:10.1016/S1534-5807(03)00162-X



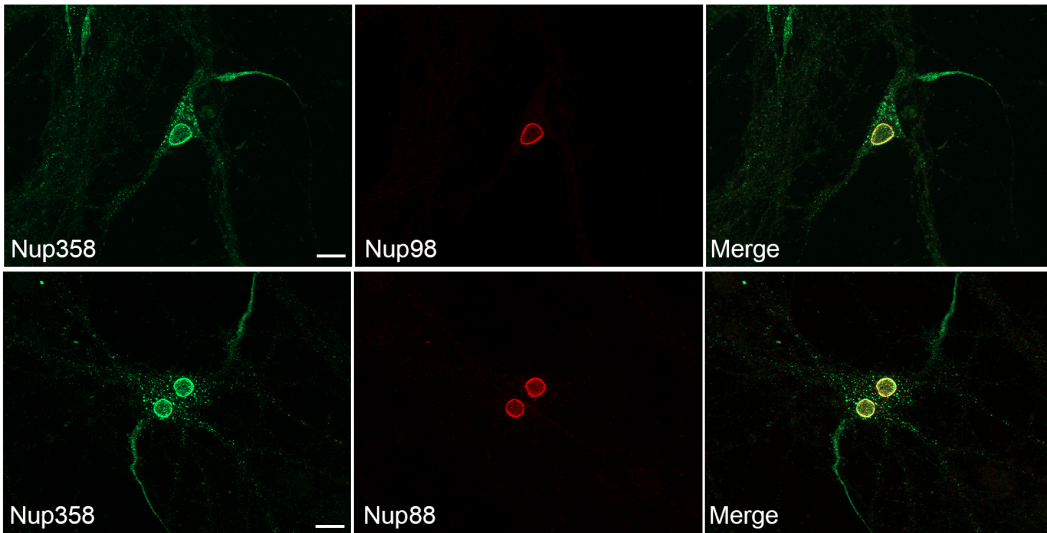
- Toda, T., Hsu, J. Y., Linker, S. B., Hu, L., Schafer, S. T., Mertens, J., Jacinto, F. V., Hetzer, M. W. and Gage, F. H.** (2017). Nup153 interacts with Sox2 to enable bimodal gene regulation and maintenance of neural progenitor cells. *Cell Stem Cell* **21**, 618-634.e7. doi:10.1016/j.stem.2017.08.012
- Vyas, P., Singh, A., Murawala, P. and Joseph, J.** (2013). Nup358 interacts with Dishevelled and aPKC to regulate neuronal polarity. *Biol. Open* **2**, 1270-1278. doi:10.1242/bio.20135363
- Winckler, B., Forscher, P. and Mellman, I.** (1999). A diffusion barrier maintains distribution of membrane proteins in polarized neurons. *Nature* **397**, 698-701. doi:10.1038/17806
- Wiznerowicz, M. and Trono, D.** (2003). Conditional suppression of cellular genes: lentivirus vector-mediated drug-inducible RNA interference. *J. Virol.* **77**, 8957-8961. doi:10.1128/JVI.77.16.8957-8951.2003
- Wu, J., Matunis, M. J., Kraemer, D., Blobel, G. and Coutavas, E.** (1995). Nup358, a cytoplasmically exposed nucleoporin with peptide repeats, Ran-GTP binding sites, zinc fingers, a cyclophilin A homologous domain, and a leucine-rich region. *J. Biol. Chem.* **270**, 14209-14213. doi:10.1074/jbc.270.23.14209
- Wu, X., Kasper, L. H., Mantcheva, R. T., Mantchev, G. T., Springett, M. J. and van Deursen, J. M. A.** (2001). Disruption of the FG nucleoporin NUP98 causes selective changes in nuclear pore complex stoichiometry and function. *Proc. Natl. Acad. Sci. U.S.A.* **98**, 3191-3196. doi:10.1073/pnas.051631598
- Wu, H.-Y., Tomizawa, K., Oda, Y., Wei, F.-Y., Lu, Y.-F., Matsushita, M., Li, S.-T., Moriwaki, A. and Matsui, H.** (2004). Critical role of calpain-mediated cleavage of calcineurin in excitotoxic neurodegeneration. *J. Biol. Chem.* **279**, 4929-4940. doi:10.1074/jbc.M309767200
- Yamada, R. and Kuba, H.** (2016). Structural and functional plasticity at the axon initial segment. *Front. Cell. Neurosci.* **10**, 250. doi:10.3389/fncel.2016.00250
- Yamashita, T., Aizawa, H., Teramoto, S., Akamatsu, M. and Kwak, S.** (2017). Calpain-dependent disruption of nucleo-cytoplasmic transport in ALS motor neurons. *Sci. Rep.* **7**, 39994. doi:10.1038/srep39994
- Yang, Q., Rout, M. P. and Akey, C. W.** (1998). Three-dimensional architecture of the isolated yeast nuclear pore complex: functional and evolutionary implications. *Mol. Cell* **1**, 223-234. doi:10.1016/S1097-2765(00)80023-4
- Yokoyama, N., Hayashi, N., Seki, T., Panté, N., Ohba, T., Nishii, K., Kuma, K., Hayashida, T., Miyata, T., Aebi, U. et al.** (1995). A giant nucleopore protein that binds Ran/TC4. *Nature* **376**, 184-188. doi:10.1038/376184a0
- Yoshimura, T. and Rasband, M. N.** (2014). Axon initial segments: diverse and dynamic neuronal compartments. *Curr. Opin. Neurobiol.* **27**, 96-102. doi:10.1016/j.conb.2014.03.004
- Zhong, G., He, J., Zhou, R., Lorenzo, D., Babcock, H. P., Bennett, V. and Zhuang, X.** (2014). Developmental mechanism of the periodic membrane skeleton in axons. *eLife* **3**, e04581. doi:10.7554/eLife.04581
- Zhou, D., Lambert, S., Malen, P. L., Carpenter, S., Boland, L. M. and Bennett, V.** (1998). Ankyrin<sub>G</sub> is required for clustering of voltage-gated Na channels at axon initial segments and for normal action potential firing. *J. Cell Biol.* **143**, 1295-1304. doi:10.1083/jcb.143.5.1295

Khalaf et al., SUPPLEMENTARY FIGURE S1

A



B



C

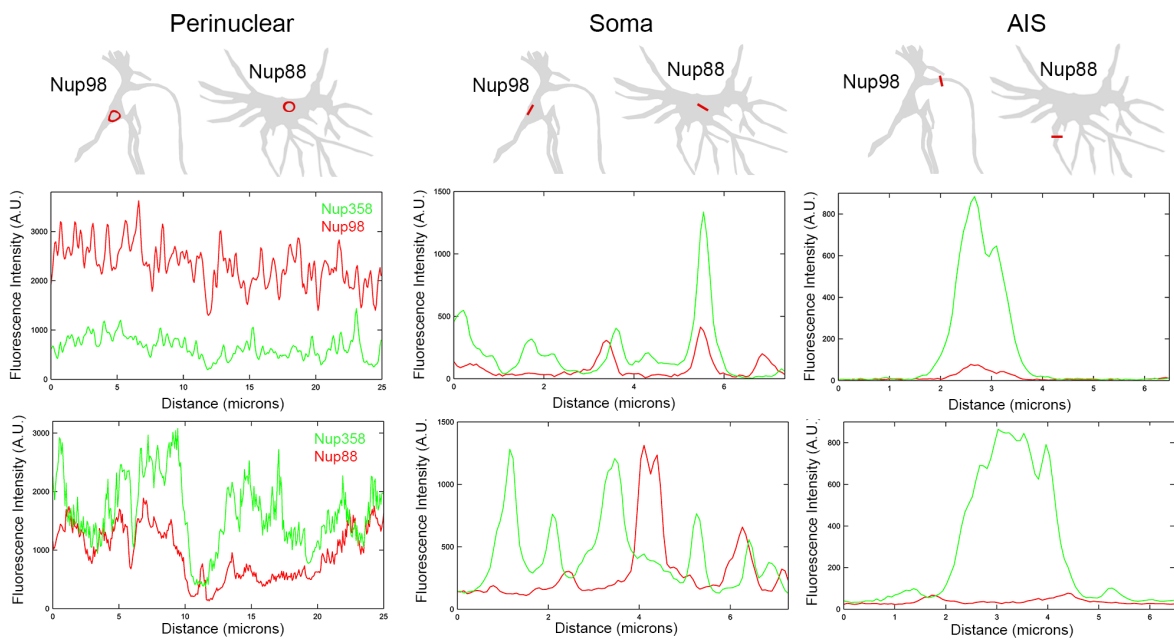
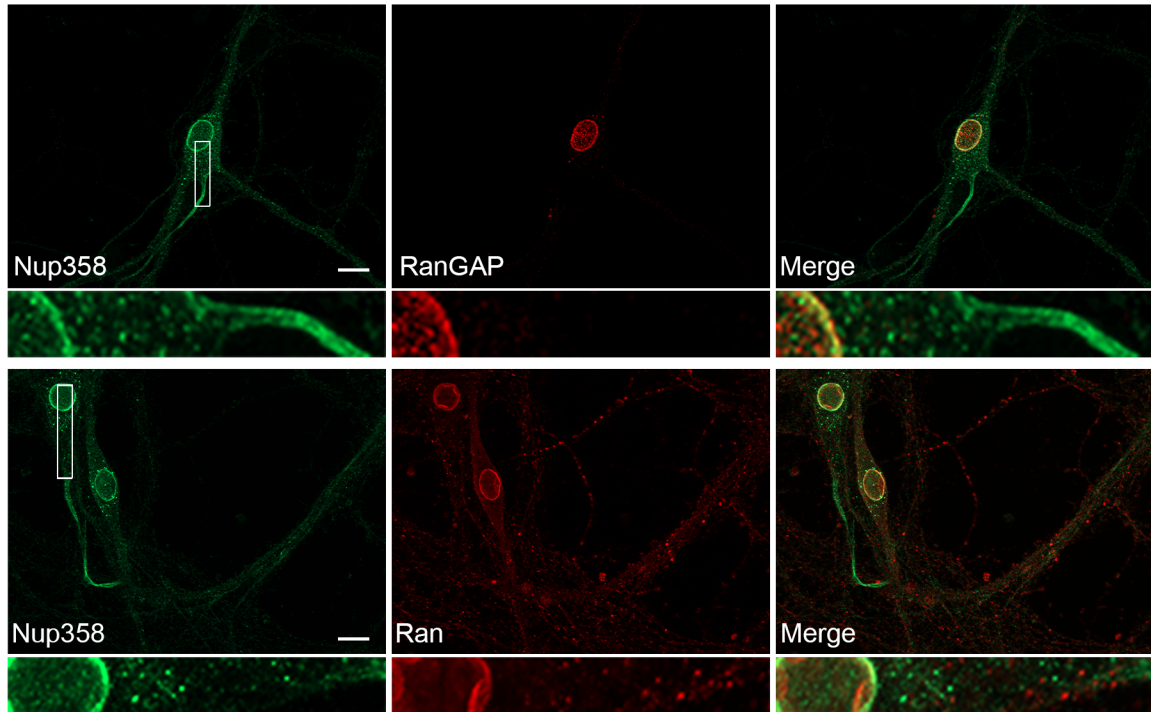


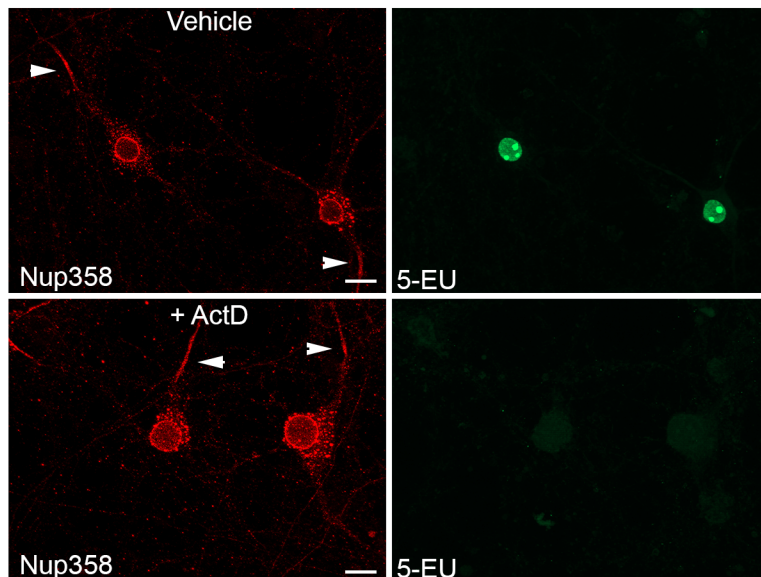
**Figure S1.** Nup358 has a unique distribution profile in neurons. **A**, 14 DIV cortical neurons immunolabeled using anti-Nup358 and anti-nuclear pore complex protein, mAb414 antibody. **B**, Fluorescent images of 14 DIV cortical neurons immunostained for Nup358 and Nup98 or Nup88. **C**, Line scan analyses of Nup358 and Nup98 or Nup88. At the top of the panel, drawings of the immunostained neurons of **B** demonstrate the locations of the lines (red lines). Nup358 is found overlapping with Nup98 and Nup88 at the perinuclear region and to a lesser extent in the soma. At the AIS, neither Nup98 nor Nup88 signals show a remarkable overlap with Nup358. Scale bar: 10  $\mu$ m.

## Khalaf et al., SUPPLEMENTARY FIGURE S2

A



B



C

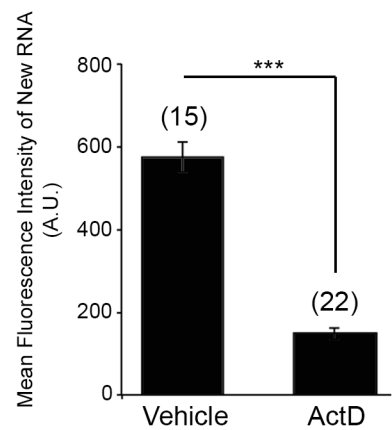


**Figure S2.** The subcellular distribution of Nup358 is distinct from that of its molecular partners and is not influenced by active RNA transcription. **A**, Immunofluorescent images of 14 DIV neurons immunostained for Nup358 and RanGAP or Ran with the magnified views showing an overlap of signals, exclusively, at the nuclear rim. **B**, Immunofluorescent images of neurons treated with DMSO (vehicle) as control or with the transcription blocker Actinomycin D (ActD; 5  $\mu$ g/ml, 1 h). 5-Ethynyl Uridine (5-EU), which is incorporated into RNA during active transcription, is detected in the control neurons while absent in the ActD-treated cells. Arrowheads are used to mark Nup358 signal at the AIS. **C**, Quantitative analysis of the mean fluorescence intensity of new RNA in vehicle versus ActD-treated neurons. 5-EU fluorescence intensity, corresponding to the new RNA, is quantified in both conditions, and the results represent means  $\pm$  s.e.m of three independent experiments with the number of cells analyzed present on top of the bars. \*\*\* $p$ <0.001 (2-tailed Student's *t*-test). Scale bar: 10  $\mu$ m.

## Khalaf et al., SUPPLEMENTARY FIGURE S3

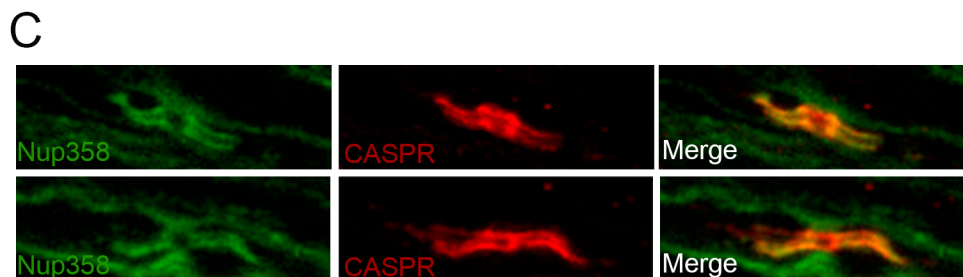
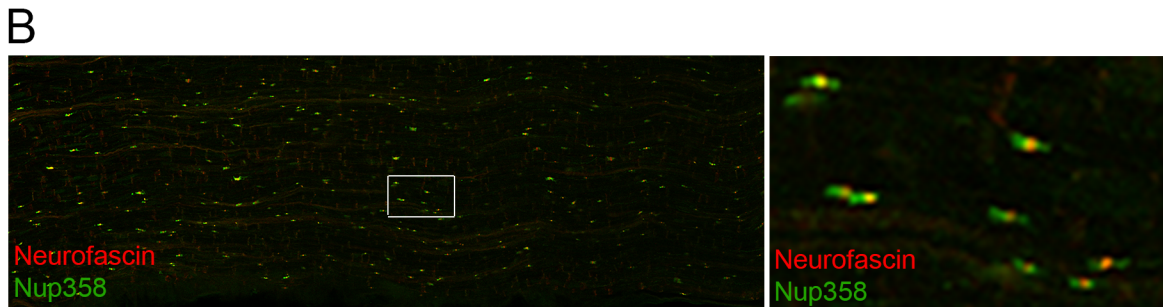
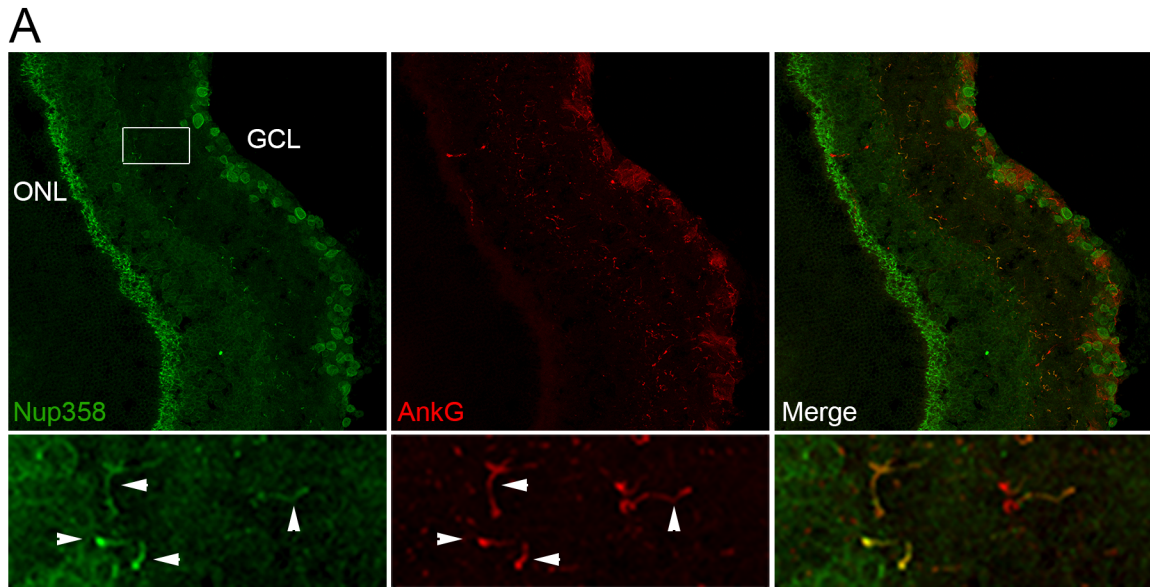


**Figure S3.** Nup358 is expressed in different tissues of the nervous system. **A**, Mouse retinal cross-section immunostained for Nup358 and AnkG. Nup358 is poorly detected in cells belonging to the outer nuclear layer (ONL), while it is prominent around nuclei of ganglion cells, labeled as the ganglion cell layer (GCL). The magnified views at the bottom of the images show a partial overlap between Nup358 and AnkG (arrowheads) in the inner plexiform layer. **B**, An immunofluorescent image of mouse sciatic nerve section stained for Nup358 and Neurofascin. The magnified view shows an overlap between Neurofascin and Nup358 signals at nodes of Ranvier, also Nup358 is being detected at the regions flanking the nodes. **C**, An image of sciatic nerve section stained for Nup358 and CASPR with the magnified view showing an overlap between both proteins at the paranodes.

## Khalaf et al., SUPPLEMENTARY FIGURE S4

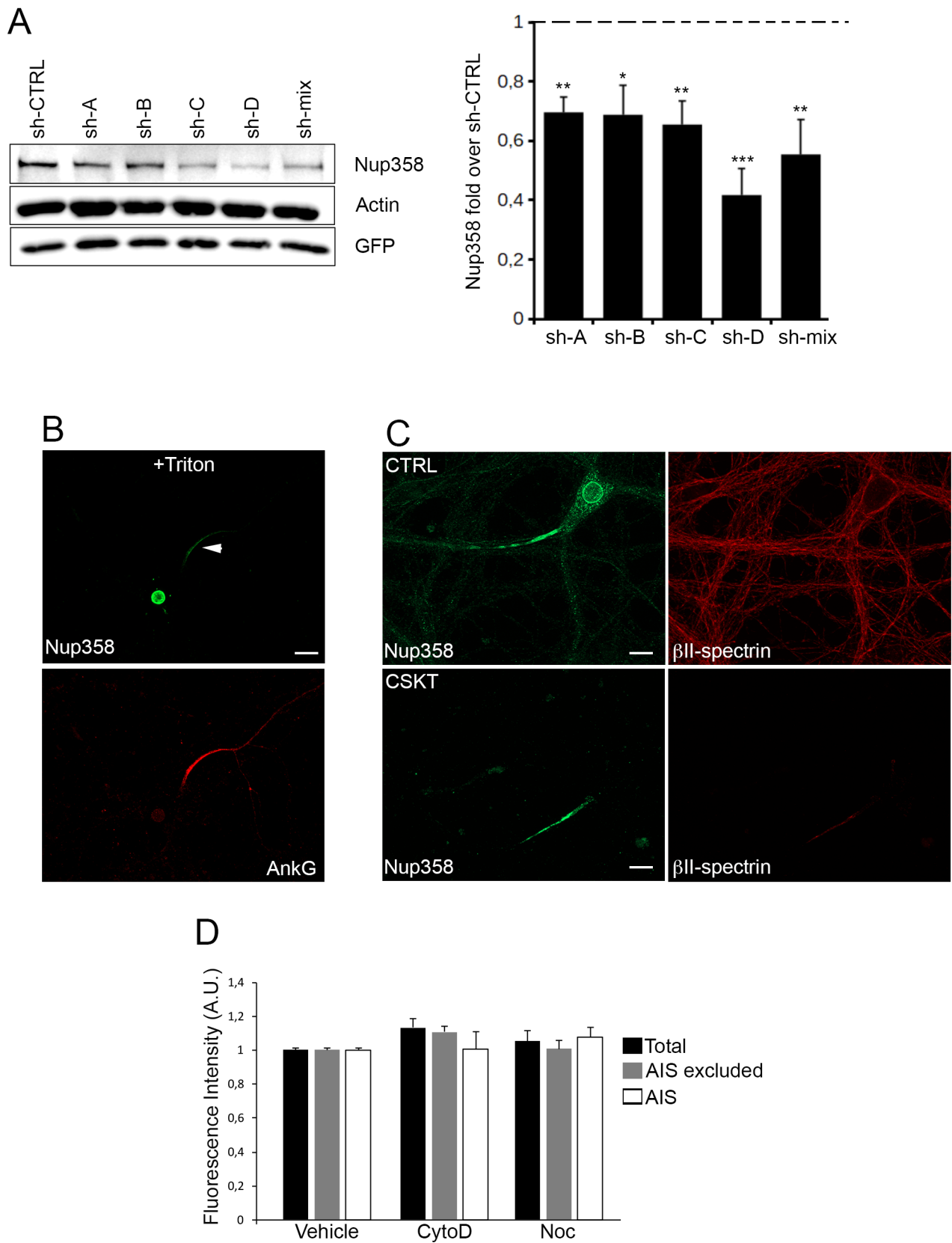




**Figure S4.** Downregulation of Nup358 in cortical neurons. **A**, Protein expression of Nup358 in cortical neurons infected with retroviruses expressing either a single (sh-A, B, C and D) or a mix of shRNAs against Nup358. A sh-RNA mismatch (sh-CTRL) was used as a control. The endogenous levels of the short form of Nup358 were analysed by Western blotting and quantified by band densitometry, with normalization to the Actin signal. Bars represent means  $\pm$  s.e.m of three independent experiments. *P*-value was calculated using 2-tailed Student's *t*-test. \* $p < 0.05$ ; \*\* $p < 0.01$ ; \*\*\* $p < 0.001$ . **B-D**, Nup358 association with the AIS is hardly affected by stringent conditions disturbing the neuronal cytoskeleton. **B**, Immunofluorescent images of 14 DIV neurons treated with 1% Triton X-100 in cytoskeletal buffer for 5 min before being fixed and immunostained for Nup358 and AnkG. The arrowhead marks the persistent signal of Nup358. **C**, Immunofluorescent images of control and detergent-extracted neurons. 14 DIV neurons were treated with 1% Triton in cytoskeletal buffer (CSKT) for 24 min, then fixed and immunostained for Nup358 and  $\beta$ II-Spectrin. Scale bar: 10  $\mu$ m. **D**, High-content analysis of Nup358 fluorescence intensity in control versus CytoD- and Noc-treated neurons ( $n > 2000$ ). 14 DIV cortical neurons were treated with any of DMSO (vehicle) as control, cytochalasin D (CytoD; 10  $\mu$ M, 1 h), or Nocodazole (Noc; 20  $\mu$ M, 3 h), after which neurons were fixed and immunostained for Nup358 and AnkG. Nup358 fluorescence intensity is measured in the entire neuronal cell (Total), in the cell body and neuronal processes excluding the AIS (AIS excluded), and at the AIS (AIS). Normalization is performed according to the values of control neurons; therefore the results represent means of relative fluorescence intensity in arbitrary unit (A.U.)  $\pm$  s.e.m of three independent experiments.  $p > 0.05$  (one-way ANOVA followed by Dunnett's post hoc test).

## Khalaf et al., SUPPLEMENTARY FIGURE S5

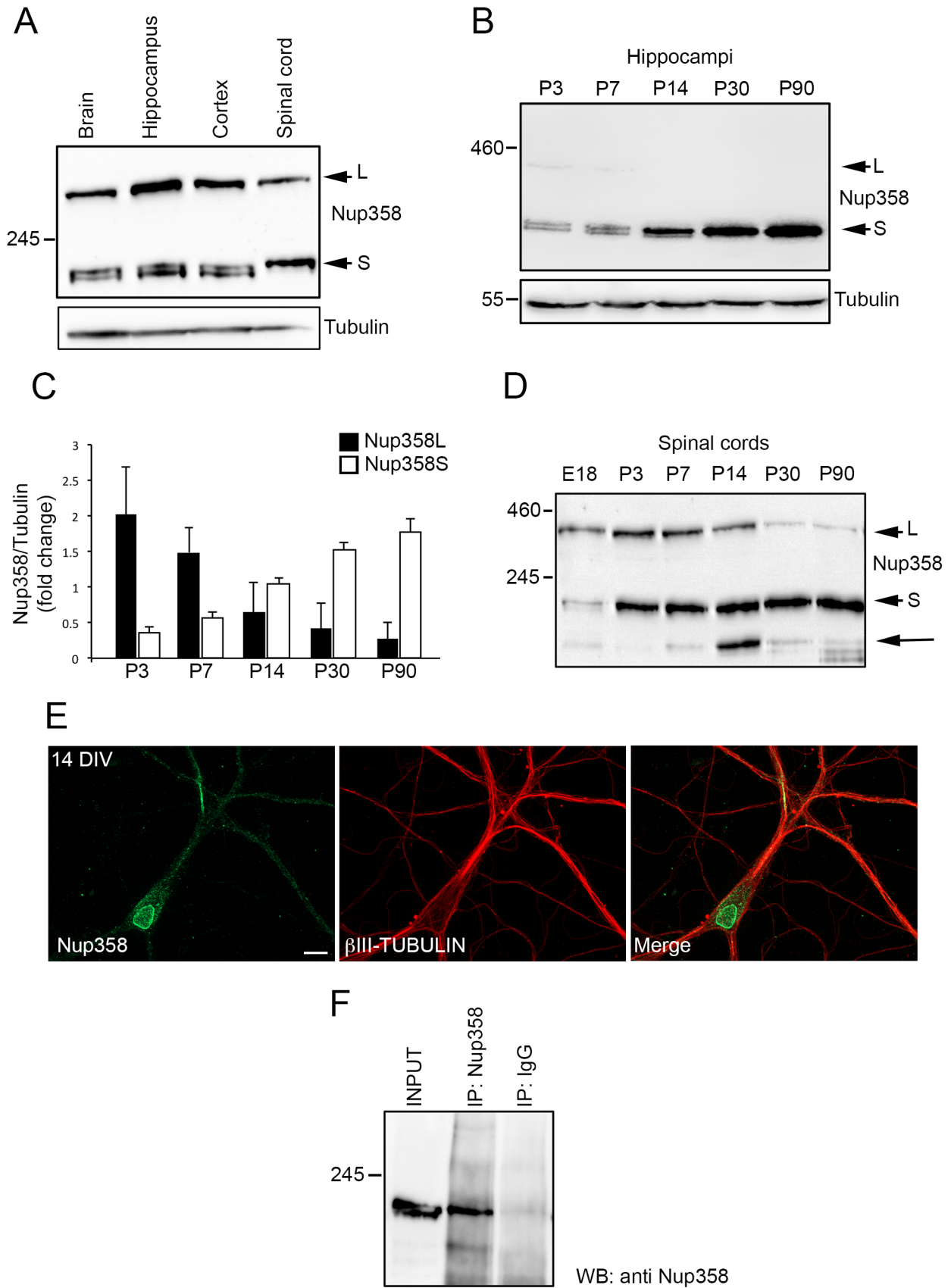


**Figure S5.** Two isoforms of Nup358 protein are expressed in the central nervous system. **A**, Immunoblot of Nup358 from samples of brain, hippocampus, cortex, and spinal cord homogenates of a P3 mouse. Two antibodies were used to detect Nup358 isoforms since each antibody has a higher affinity for a specific isoform. Tubulin serves as a loading control. **B** and **C**, Development-dependent changes in expression of Nup358 isoforms in hippocampi. Hippocampal samples were obtained from mice at the embryonic day (E18) and the postnatal period (P3-P90), and immunoblotted for Nup358, and Tubulin as a loading control. **C**, Quantitative analysis of Nup358 isoforms/Tubulin ratios in the developing hippocampus. The results shown are means  $\pm$  s.e.m of three independent experiments. **D**, Immunoblot of Nup358 from samples of spinal cords throughout development from E18-P90. In **A-D**, arrowheads mark the expression of Nup358L and Nup358S. The arrow in **D** is directed toward an unidentified band running slightly lower than the 230 kDa band in the P14 mouse spinal cord. **E**, Fluorescent images of 14 DIV hippocampal neuron immunolabeled for Nup358 and  $\beta$ III-tubulin. Scale bar: 10  $\mu$ m. **F**, Immunoblot of Nup358 from P30 mouse cortex showing the short form of Nup358 in the Input and the immunoprecipitated (IP: Nup358) samples while absent in the control (IP: IgG) sample.

# Khalaf et al., SUPPLEMENTARY FIGURE S6

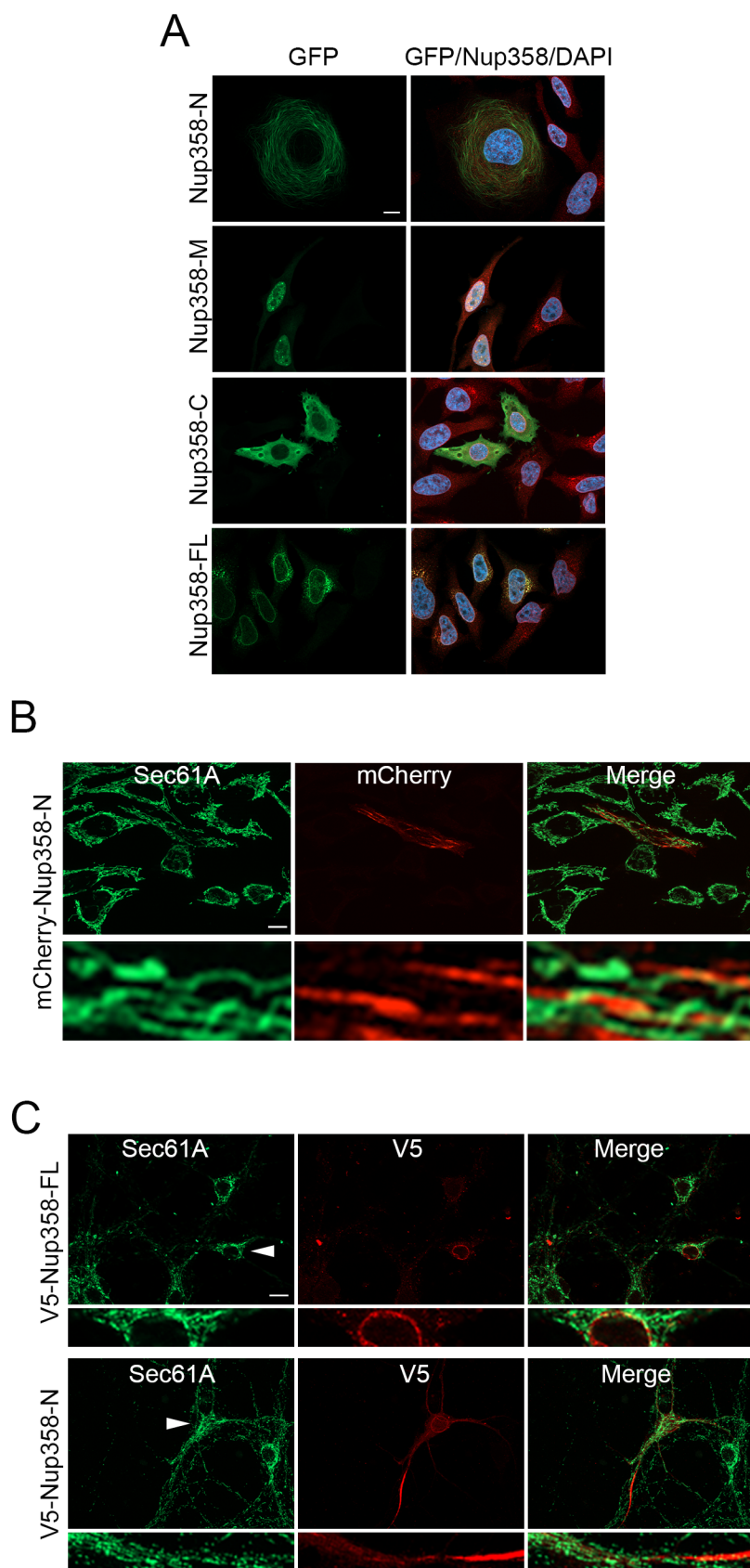
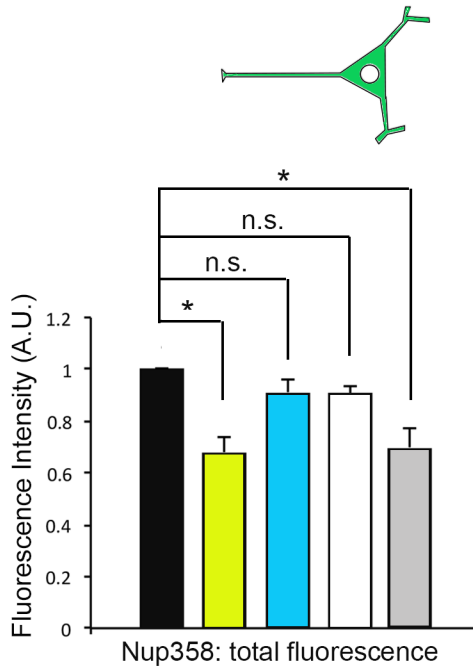


**Figure S6.** Transient expression of Nup358 in HeLa cell line and 9 DIV neurons. **A**, Immunofluorescent images of HeLa cells transfected with constructs expressing different regions of Nup358: GFP-Nup358-N (1-900 amino acids), GFP-Nup358-M (901-2219), GFP-Nup358-C (2220-3224), or with a construct encoding for the entire human Nup358 protein GFP-Nup358-FL (1-3224 amino acids). HeLa cells were then immunostained for endogenous Nup358 (red), and cell nuclei were identified by DAPI staining. **B**, Fluorescent images of HeLa cells transfected with mCherry-Nup358-N and immunostained for the endoplasmic reticulum marker, Sec61A. **C**, Fluorescent images of 9 DIV cortical neurons transfected with V5 co-expressing constructs, namely V5-Nup358-FL or V5-Nup358-N. Neurons were immunostained for Sec61A. Arrowheads are used to mark the transfected neurons with magnified views shown at the bottom of the images. Scale bar: 10  $\mu$ m.

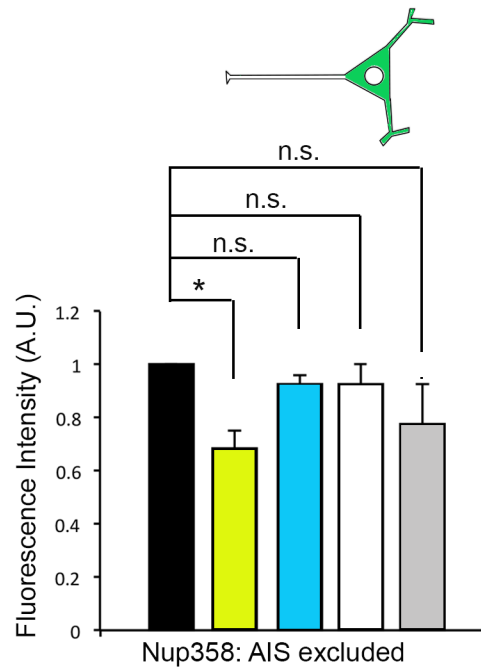
# Khalaf et al., SUPPLEMENTARY FIGURE S7

NaCl   
  KCl   
  KCl+EGTA   
  KCl+APV   
  KCl+CNQX

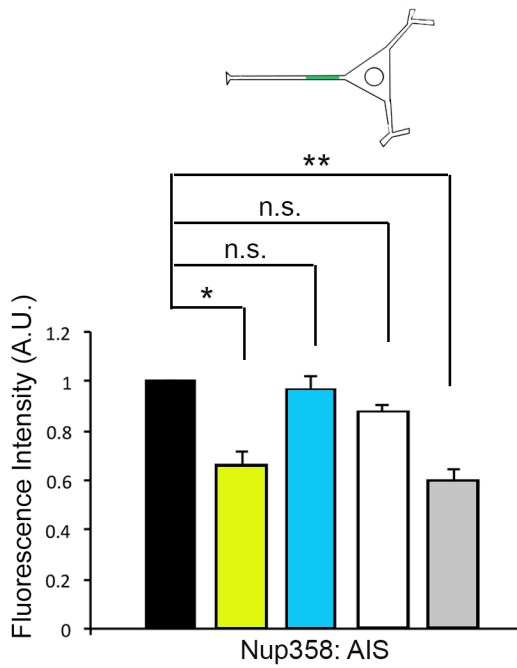
**A**



**B**



**C**



**D**

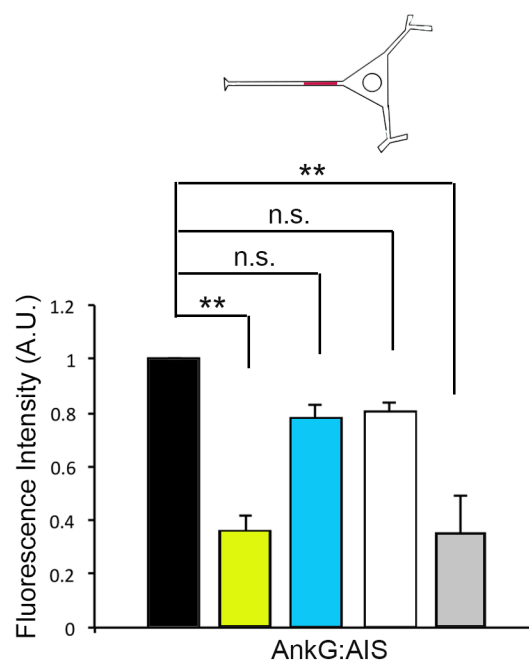
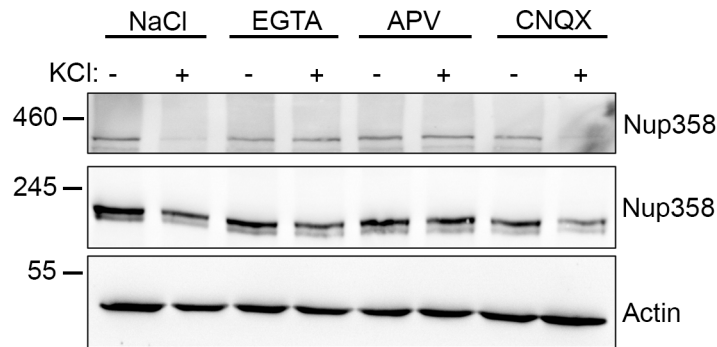


**Figure S7.** KCl-treatment reduces Nup358 expression in neurons, mediated by activation of NMDA receptors and increased Calcium influx. **A-D**, 14 DIV cortical neurons were treated with KCl alone (50 mM, 1 h), or together with EGTA (2 mM, 30 min), APV (50  $\mu$ M, 30 min), or CNQX (40  $\mu$ M, 30 min); neurons treated with NaCl serve as control. Nup358 or AnkG fluorescence intensity was quantified and normalized to the intensity in the NaCl-treated cells thus represented as relative fluorescence intensity (A.U.). A schematic drawing of the neuronal cell accompanies each histogram to demonstrate the region selected for the analysis (colored in green or red). **A**, Nup358 fluorescence intensity in the entire neuronal cell, depicted as “Nup358: total fluorescence”. **B**, Nup358 fluorescence intensity in the neuronal cells but excluding Nup358 pool at the AIS, thus denoted as “Nup358: AIS excluded”. **C**, Nup358 fluorescence intensity at the level of the AIS, thus denoted as “Nup358: AIS”. **D**, AnkG fluorescence intensity is indicated as “AnkG: AIS”. The results presented are means  $\pm$  s.e.m. of three independent experiments. \* $p < 0.05$ , \*\* $p < 0.01$ , and n.s. represents non-significant values (one-way ANOVA followed by Dunnett’s post hoc test).

## Khalaf et al., SUPPLEMENTARY FIGURE S8

A



B

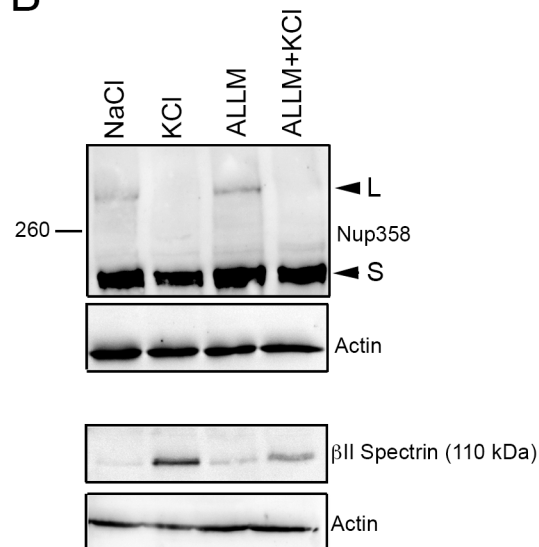


**Figure S8.** NMDARs, Calcium entry and Calpain activation are key players in the KCl-mediated decrease in Nup358 expression. **A**, Immunoblot of full-length and short forms of Nup358 from 14 DIV cortical neurons treated with KCl (50 mM, 1 h) and/or EGTA (2 mM, 30 min), APV (50  $\mu$ M, 30 min), and CNQX (40  $\mu$ M, 30 min); neurons treated with NaCl were used as control. Actin serves as a loading control. The marks (-) or (+) are used to indicate when KCl is included in treatments or not. **B**, Immunoblot of Nup358 and  $\beta$ II-Spectrin from 14 DIV cortical neurons treated with KCl (50 mM) and/or the calpain inhibitor ALLM (25  $\mu$ M, 30 min). Neurons treated with NaCl represent the control. Arrowheads mark the expression of Nup358 isoforms. Notably, a cleaved form of  $\beta$ II-Spectrin (110 kDa) is detected in the KCl-treated neurons. Actin serves as a loading control.



TABLE S1

Identified Proteins	Accession Number	Molecular Weight	Exclusive Unique Peptide Count
ADP/ATP translocase 1 OS=Mus musculus GN=Slc25a4 PE=1 SV=4	ADT1_MOUSE	33 kDa	3
ARF6 guanine nucleotide exchange factor IQArfGEF OS=Mus musculus GN=Iqsec2 PE=1 SV=1	A4G226_MOUSE (+3)	162 kDa	28
Actin, cytoplasmic 2 OS=Mus musculus GN=Actg1 PE=1 SV=1	ACTG_MOUSE	42 kDa	5
<b>Ankyrin-3 (Fragment) OS=Mus musculus GN=Ank3 PE=4 SV=1</b>	S4R2K9_MOUSE	285 kDa	22
Calcium/calmodulin-dependent protein kinase type II subunit alpha OS=Mus musculus GN=Camk2a PE=1 SV=2	sp P11798 KCC2A_MOUSE	54 kDa	6
Calmodulin-regulated spectrin-associated protein 2 OS=Mus musculus GN=Camsap2 PE=1 SV=1	A0A0AGY67_MOUSE (+3)	166 kDa	5
Centrosomal protein of 170 kDa protein B OS=Mus musculus GN=Cep170b PE=1 SV=2	sp Q80U49 C170B_MOUSE	171 kDa	18
Clathrin heavy chain 1 OS=Mus musculus GN=Cltc PE=1 SV=3	CLH1_MOUSE (+1)	192 kDa	11
<b>E3 SUMO-protein ligase RanBP2 OS=Mus musculus GN=Ranbp2 PE=1 SV=2</b>	RBP2_MOUSE	341 kDa	40
Excitatory amino acid transporter 2 OS=Mus musculus GN=Slc1a2 PE=1 SV=1	sp P43006 EAA2_MOUSE	62 kDa	3
Glutamate receptor ionotropic, NMDA 1 OS=Mus musculus GN=Grin1 PE=4 SV=1	A2AI21_MOUSE (+1)	108 kDa	4
Glutamate receptor ionotropic, NMDA 2B OS=Mus musculus GN=Grin2b PE=1 SV=1	G3X9V4_MOUSE (+1)	166 kDa	7
Glyceraldehyde-3-phosphate dehydrogenase OS=Mus musculus GN=Gapdh PE=1 SV=1	A0A0A0MQF6_MOUSE (+1)	39 kDa	4
Histone H4 OS=Mus musculus GN=Hist1h4 PE=1 SV=2	H4_MOUSE	11 kDa	3
Isoform 2 of Caskin-1 OS=Mus musculus GN=Caskin1	sp Q6P9K8-2 CSK11_MOUSE (+1)	143 kDa	5
Isoform 2 of Protein piccolo OS=Mus musculus GN=Pclo	sp Q9YQX7-2 PCLO_MOUSE (+1)	528 kDa	17
Isoform 2 of Reticulon-4 OS=Mus musculus GN=Rtn4	sp Q99P72-3 RTN4_MOUSE (+1)	114 kDa	7
Isoform 2 of Signal-induced proliferation-associated 1-like protein 1 OS=Mus musculus GN=Sipa11	sp Q8C0T5-2 S1L1_MOUSE (+1)	193 kDa	13
Isoform 3 of Glutamate receptor 2 OS=Mus musculus GN=Gria2	sp P23819-3 GRIA2_MOUSE (+1)	105 kDa	4
Isoform 3 of Regulating synaptic membrane exocytosis protein 1 OS=Mus musculus GN=Rims1	sp Q99NE5-3 RIMS1_MOUSE (+1)	160 kDa	30
Isoform 7 of Regulating synaptic membrane exocytosis protein 1 OS=Mus musculus GN=Rims1	sp Q99NE5-7 RIMS1_MOUSE	133 kDa	6
Kalirin OS=Mus musculus GN=Kalrn PE=1 SV=1	A0A0A0MQF1_MOUSE (+6)	219 kDa	7
Laminin subunit beta-2 OS=Mus musculus GN=Lamb2 PE=2 SV=2	LAMB2_MOUSE	197 kDa	9
Leucine-rich repeat-containing protein 7 OS=Mus musculus GN=Lrrc7 PE=1 SV=1	E9Q6L9_MOUSE (+1)	173 kDa	15
Microtubule-associated protein 1A OS=Mus musculus GN=Map1a PE=1 SV=1	A2ARP8_MOUSE (+2)	326 kDa	3
Microtubule-associated protein 2 OS=Mus musculus GN=Map2 PE=1 SV=2	MTAP2_MOUSE	199 kDa	3
Myelin proteolipid protein OS=Mus musculus GN=Pmp1 PE=1 SV=2	sp P60202 MYPR_MOUSE	30 kDa	4
Myo18a protein OS=Mus musculus GN=Myo18a PE=1 SV=1	B2RRE2_MOUSE (+5)	232 kDa	3
Myosin-9 OS=Mus musculus GN=Myh9 PE=1 SV=4	MYH9_MOUSE	226 kDa	3
Myosin-10 OS=Mus musculus GN=Myh10 PE=1 SV=2	MYH10_MOUSE (+1)	229 kDa	18
Neural cell adhesion molecule 1 OS=Mus musculus GN=Ncam1 PE=1 SV=3	sp P13595 NCAM1_MOUSE	119 kDa	5
<b>Neurofascin OS=Mus musculus GN=Nfasc PE=1 SV=1</b>	NFASC_MOUSE	138 kDa	38
Neurofilament heavy polypeptide OS=Mus musculus GN=Nefh PE=1 SV=3	NFH_MOUSE	117 kDa	19
Neurofilament medium polypeptide OS=Mus musculus GN=Nefm PE=1 SV=4	NFM_MOUSE	96 kDa	10
Plasma membrane calcium-transporting ATPase 2 OS=Mus musculus GN=Atp2b2 PE=1 SV=2	AT2B2_MOUSE (+2)	133 kDa	4
Plectin OS=Mus musculus GN=Plec PE=1 SV=1	E9Q3W4_MOUSE (+16)	499 kDa	5
Protein Lmo7 OS=Mus musculus GN=Lmo7 PE=1 SV=1	E9PYF4_MOUSE (+2)	193 kDa	9
Protein Raph1 OS=Mus musculus GN=Raph1 PE=1 SV=2	F2Z3U3_MOUSE	137 kDa	4
Protein Slc8a2 OS=Mus musculus GN=Slc8a2 PE=2 SV=1	Q8K596_MOUSE	101 kDa	3
Protein Sptbn2 OS=Mus musculus GN=Sptbn2 PE=1 SV=1	Q68FG2_MOUSE	271 kDa	6
Protein Zscan18 OS=Mus musculus GN=Zscan18 PE=4 SV=1	E9PUD6_MOUSE	92 kDa	11
Protein bassoon OS=Mus musculus GN=Bsn PE=1 SV=4	sp O88737 BSN_MOUSE	419 kDa	39
Protein unc-13 homolog A OS=Mus musculus GN=Unc13a PE=1 SV=1	H3BJZ7_MOUSE (+1)	196 kDa	9
Rap guanine nucleotide exchange factor 2 OS=Mus musculus GN=Rapgef2 PE=1 SV=1	A0A0AGYWG7_MOUSE (+2)	184 kDa	7
SH3 and multiple ankyrin repeat domains protein 1 OS=Mus musculus GN=Shank1 PE=1 SV=1	D3YZU4_MOUSE (+2)	225 kDa	5
SH3 and multiple ankyrin repeat domains protein 2 OS=Mus musculus GN=Shank2 PE=1 SV=1	D3Z5K9_MOUSE (+2)	159 kDa	30
SH3 and multiple ankyrin repeat domains protein 3 OS=Mus musculus GN=Shank3 PE=1 SV=1	sp Q4ACU6 SHAN3_MOUSE	185 kDa	7
Sodium/potassium-transporting ATPase subunit alpha-1 OS=Mus musculus GN=Atp1a1 PE=1 SV=1	AT1A1_MOUSE	113 kDa	3
Sodium/potassium-transporting ATPase subunit alpha-2 OS=Mus musculus GN=Atp1a2 PE=1 SV=1	AT1A2_MOUSE (+1)	112 kDa	3
Sodium/potassium-transporting ATPase subunit alpha-3 OS=Mus musculus GN=Atp1a3 PE=1 SV=1	AT1A3_MOUSE (+1)	112 kDa	15
Sorbin and SH3 domain-containing protein 1 OS=Mus musculus GN=Sorbs1 PE=1 SV=2	sp Q62417 SRBS1_MOUSE	143 kDa	7
Spectrin alpha chain, non-erythrocytic 1 OS=Mus musculus GN=Sptan1 PE=1 SV=1	A3KGU7_MOUSE	285 kDa	20
Spectrin beta chain, non-erythrocytic 1 OS=Mus musculus GN=Sptbn1 PE=1 SV=2	sp Q62261 SPTB2_MOUSE	274 kDa	18
Synaptic vesicle glycoprotein 2A OS=Mus musculus GN=Sv2a PE=1 SV=1	SV2A_MOUSE	83 kDa	3
Tenascin-R OS=Mus musculus GN=Tnr PE=1 SV=2	sp Q8BYI9 TENR_MOUSE	150 kDa	9
Tubulin alpha-1A chain OS=Mus musculus GN=Tuba1a PE=1 SV=1	TBA1A_MOUSE (+1)	50 kDa	6
Unconventional myosin-Va OS=Mus musculus GN=Myo5a PE=1 SV=1	D3YZ62_MOUSE (+1)	212 kDa	67
V-type proton ATPase subunit a OS=Mus musculus GN=Atp6v0a1 PE=1 SV=1	K3W4T3_MOUSE (+3)	96 kDa	6

**Nup358 vs IgG**

Identified Proteins	Accession Number	Molecular Weight	IgG Control	Nup358 IP
Actin, cytoplasmic 1 OS=ACTB	ACTB_BOVIN (+20)	42 kDa	3	11
Actin, cytoplasmic 2 OS=actg1	ACTG_RANLE	42 kDa	4	11
Alpha-internexin OS=Ina	AIX_MOUSE	56 kDa	0	3
Ankyrin-2 OS=Ank2	ANK2_MOUSE	426 kDa	0	2
<b>Ankyrin-3 OS=ANK3</b>	ANK3_HUMAN	480 kDa	0	3
ATP synthase subunit beta, mitochondrial OS=Atp5b	ATPB_MOUSE	56 kDa	0	3
Calcium/calmodulin-dependent protein kinase type II subunit beta OS=CAMK2B	KCC2B_HUMAN (+2)	73 kDa	0	3
DESM_MOUSE-DECOY	DESM_MOUSE-DECOY	?	0	2
Drebrin OS=DBN1	DREB_HUMAN (+2)	71 kDa	0	2
<b>E3 SUMO-protein ligase RanBP2</b>	RBP2_HUMAN	358 kDa	0	2
EF-hand domain-containing protein D2 OS=Efh2	EFHD2_MOUSE	27 kDa	1	2
Enhancer of mRNA-decapping protein 4 OS=Edc4	EDC4_MOUSE	152 kDa	0	6
Myelin basic protein OS=Mbp	MBP_MOUSE	27 kDa	4	3
Myosin-XVIIla OS=Myo18a	MY18A_MOUSE	233 kDa	0	4
Protein bassoon OS=Bsn	BSN_MOUSE	419 kDa	0	6
Protein FAM179B OS=FAM179B	F179B_HUMAN	189 kDa	2	0
Protein piccolo OS=Pclo	PCLO_MOUSE	548 kDa	0	2
Ran GTPase-activating protein 1 OS=Rangap1	RAGP1_MOUSE	64 kDa	0	3
Ras GTPase-activating protein SynGAP OS=Syngap1	SYGP1_RAT	145 kDa	0	4
Receptor expression-enhancing protein 1 OS=Reep1	REEP1_MOUSE	22 kDa	0	3
Rho guanine nucleotide exchange factor 18 OS=Arhgef18	ARHG1_MOUSE	114 kDa	0	2
SH3 and multiple ankyrin repeat domains protein 1 OS=Shank1	SHAN1_RAT	226 kDa	0	2
SH3 and multiple ankyrin repeat domains protein 3 OS=Shank3	SHAN3_MOUSE	192 kDa	0	4
Sodium/potassium-transporting ATPase subunit alpha-1 OS=Atp1a1	AT1A1_MOUSE (+1)	113 kDa	0	3
Spectrin alpha chain, brain OS=GN=Sptan1	SPTA2_MOUSE (+1)	285 kDa	2	3
Spectrin beta chain, brain 1 OS=Sptbn1	SPTB2_MOUSE	274 kDa	0	3

SRC kinase signaling inhibitor 1 OS=Srcin1	SRCN1_MOUSE	135 kDa	0	2
Synaptosomal-associated protein 25 OS=SNAP25	SNP25_BOVIN (+7)	23 kDa	0	4
Syntaxin-1B OS=STX1B	STX1B_BOVIN (+4)	33 kDa	0	2
Transitional endoplasmic reticulum ATPase OS=VCP	TERA_BOVIN (+7)	89 kDa	0	2
Tubulin alpha-1A chain OS=TUBA1A	TBA1A_CRIGR [27]	50 kDa	1	6
Tubulin alpha-4A chain OS=TUBA4	TBA4A_BOVIN (+4)	50 kDa	1	3
V-type proton ATPase subunit B, brain isoform OS=ATP6V1B2	VATB2_BOVIN (+4)	57 kDa	0	2
V-type proton ATPase subunit E 1 OS=ATP6V1E1	VATE1_BOVIN (+4)	26 kDa	0	2
Vesicle-associated membrane protein 2 OS=Vamp2	VAMP2_MOUSE (+1)	13 kDa	1	4

**Table S1.** List of proteins identified with immunoprecipitated Nup358. Highlighted in bold are the AIS proteins Ankyrin-G (Ank3) and Neurofascin, together with Nup358 (E3 SUMO-protein ligase RanBP2). The table shows all identified proteins with their accession numbers, molecular weight and the number of exclusive unique peptides for each protein.